A COMPARISON OF FAULT DETECTION METHODS FOR A TRANSCRITICAL REFRIGERATION SYSTEM

A Thesis

by

ALEX KARL JANECKE

Submitted to the Office of Graduate Studies of
Texas A&M University
in partial fulfillment of the requirements for the degree of

MASTER OF SCIENCE

August 2011

Major Subject: Mechanical Engineering

A COMPARISON OF FAULT DETECTION METHODS FOR A TRANSCRITICAL REFRIGERATION SYSTEM

A Thesis

by

ALEX KARL JANECKE

Submitted to the Office of Graduate Studies of
Texas A&M University
in partial fulfillment of the requirements for the degree of

MASTER OF SCIENCE

Approved by:

Chair of Committee,	Bryan Rasmussen
Committee Members,	Alexander Parlos
	Juergen Hahn
Head of Department,	Dennis O'Neal

August 2011

Major Subject: Mechanical Engineering

ABSTRACT

A Comparison of Fault Detection Methods for a Transcritical Refrigeration System.

(August 2011)

Alex Karl Janecke, B.S., Texas A&M University

Chair of Advisory Committee: Dr. Bryan Rasmussen

When released into the atmosphere, traditional refrigerants contribute to climate change several orders of magnitude more than a corresponding amount of carbon dioxide. For that reason, an increasing amount of interest has been paid to transcritical vapor compression systems in recent years, which use carbon dioxide as a refrigerant. Vapor compression systems also impact the environment through their consumption of energy. This can be greatly increased by faulty operation. Automated techniques for detecting and diagnosing faults have been widely tested for subcritical systems, but have not been applied to transcritical systems. These methods can involve either dynamic analysis of the vapor compression cycle or a variety of algorithms based on steady state behavior.

In this thesis, the viability of dynamic fault detection is tested in relation to that of static fault detection for a transcritical refrigeration system. Step tests are used to determine that transient behavior does not give additional useful information. The same tests are performed on a subcritical air conditioner showing little value in dynamic fault detection. A static component based method of fault detection which has been applied to

subcritical systems is also tested for all pairings of four faults: over/undercharge, evaporator fouling, gas cooler fouling, and compressor valve leakage. This technique allows for low cost measurement and independent detection of individual faults even when multiple faults are present. Results of this method are promising and allow distinction between faulty and fault-free behavior.

ACKNOWLEDGEMENTS

I would like to thank my advisor Dr. Rasmussen for all the help and advice he has given during my time in graduate school. Without his guidance this thesis would not be possible. I would like to thank Dr. Parlos and Dr. Hahn for serving on my committee. All of my colleagues in the Thermofluids Controls Lab deserve thanks for putting up with me over the last two years and making my time in graduate school much more enjoyable. I would like to thank Danfoss Saginomiya and Sensata for freely supplying parts for my project. Finally and most importantly, I would like to thank my family for all the support they have given me through my college career.

NOMENCLATURE

A_i	Internal pipe wall area
A_o	External pipe wall area
C_d	Coefficient of discharge
$c_{p,a}$	Specific heat of air
$\dot{E}_w$	Rate of change of wall energy
$E(t)$	Error signal
h	Enthalpy
k	Compressor coefficient/thermal conductivity
$k_{sc,sh}$	Empirical constant
$\dot{m}$	Mass flow rate
n	Number of nodes in FCV model/compressor coefficient
P	Pressure
$\dot{Q}_{loss}$	Compressor heat loss
T	Temperature
$\dot{U}$	Rate of change of refrigerant energy
u	Input vector FCV model
u_{valve}	Valve input
v	Valve coefficient
$\dot{W}_{comp}$	Compressor power

x	State vector FCV model
α	Heat transfer coefficient/charge sensor coefficient
β	Empirical coefficient
ρ	Density
ΔC	Transcritical charge indicator
ΔT_{sh-sc}	Subcritical charge fault indicator
ΔT_{kro}	Compressor valve leakage indicator
$Z(x,u)$	Matrix for FCV model
$f(x,u)$	Input vector for FCV model

Subscripts

a	Air
c	Compressor
e	Evaporator
gc	Gas cooler
hx	Heat exchanger
i	Internal
k	Indexing variable
n	Number of nodes in FCV model
o	External
r	Refrigerant
sh	Superheat

sc	Subcooling
v	Valve
w	Pipe wall
est	Estimated
in	Inlet
out	Outlet
nom	Nominal

TABLE OF CONTENTS

Page

LIST OF FIGURES

FIGURE Page

FIGURE Page

LIST OF TABLES

INTRODUCTION

As of 2001 the Department of Energy estimated that the percentage of household electricity usage for air conditioners, refrigerators, and freezers exceeded 30% [1]. With such a large proportion of energy consumption being used by HVAC&R systems, maximizing energy efficiency has become an important field of study. Estimates of the waste caused by degradation of equipment or improper commissioning run as high as 15 to 30% [2].

A variety of faulty behaviour can occur in HVAC equipment. These faults can be present at the installation of the system, accumulate gradually over time, or happen abruptly. Unlike other fields, there is generally no safety risk in these faulty conditions. Instead fault detection and diagnosis (FDD) will benefit the system through reduced energy consumption and lower maintenance costs; therefore, any successful algorithm for FDD must be not only accurate but low in cost.

Vapor compression cycles raise environmental concerns beside their energy use. According to the Intergovernmental Panel on Climate Change, eleven of the twelve years between 1995 and 2006 ranked with the highest temperatures since direct measurement has been available [3]. The use of hydroflourocarbons (HFCs) as refrigerants contributes to climate change. Global warming potential (GWP) is a measure of how much a given substance affects climate change when released in the atmosphere. The baseline value of one is given to one kilogram of carbon dioxide.

This thesis follows the style of *IEEE Transactions on Control Systems Technology*.

Table 1 shows the GWP given to the most common refrigerants as determined by the EPA [4].

Table 1. GWP of common refrigerants

Refrigerant	GWP
R-134a	1300
R-410	1725
R744 (CO_2)	1

Because of the value in pursuing carbon dioxide as an alternative refrigerant, this thesis seeks to investigate different techniques for FDD within a carbon dioxide refrigeration system. Testing will be done to determine what dynamic models may add to the accuracy and reliability of static FDD techniques. Also a leading static method of FDD will be tested on the carbon dioxide system as well as a more traditional subcritical air conditioner using R410. Emphasis will be placed on the changes necessary for this method to function properly in the transcritical cycle, which is used in carbon dioxide based systems.

The Subcritical and Transcritical Cycles

The subcritical vapor compression cycle consists of four steps. In the first a refrigerant is compressed so that it will have a high pressure and temperature. The second step involves an isobaric cooling of this vapor in the condenser until it is a liquid. In the third step the refrigerant then enters a valve where it undergoes isentropic

expansion becoming a two-phase fluid. Finally, in the fourth step the refrigerant receives isobaric heating in the evaporator leaving as a superheated vapor.

The transcritical cycle differs from the subcritical cycle in one important way. In the subcritical cycle the condenser cools the refrigerant leaving the compressor taking it from a gas to a two-phase fluid and generally to a pure liquid. In a transcritical cycle, however, the discharge pressure of the compressor is higher than the critical point of the refrigerant. Because there is no two-phase fluid the heat exchanger in which the cooling of the refrigerant after compression takes place is called a gas cooler instead of a condenser. Figure 1 shows the subcritical and transcritical cycles on a *p-h* diagram.

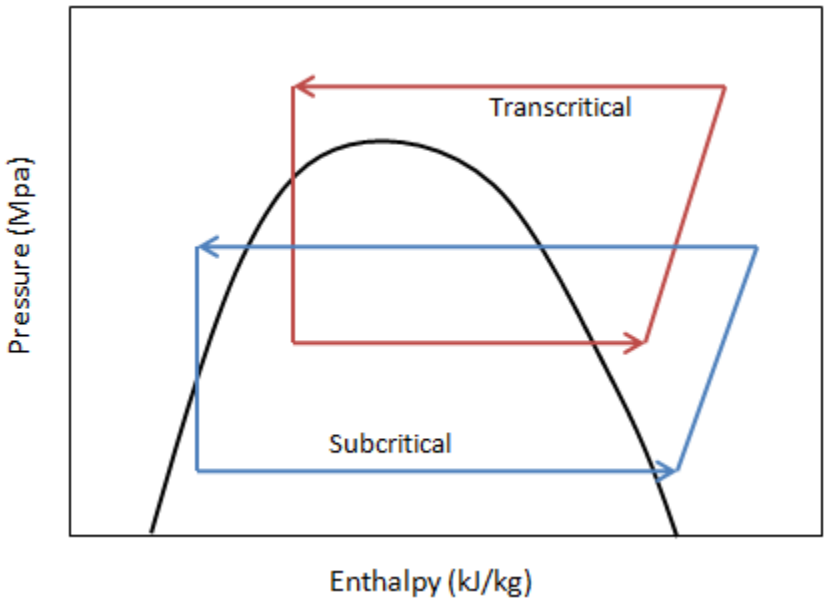

Figure 1. Subcritical and transcritical cycles

Literature Review

The emergence of FDD in HVAC is a more recent trend. Comstock et al. surveyed manufacturers of chiller systems to estimate the cost and incidence of faults and failures in the field [5]. Katipamula and Brambley provided a two-part survey of different FDD techniques applied to air-conditioning and refrigeration systems for building units [2, 6]. In the first part techniques were classified as either qualitative or quantitative. In part two algorithms from the literature on HVAC systems are compared.

Dynamic Fault Detection

Dynamic fault detection uses transient data and models to find and identify faulty system behavior. Dynamic fault detection arose as a field in the 1970's. Wilsky summarized many of the early fault detection and diagnosis (FDD) schemes used [7]. Clark gave an early observer based method with the example of a hydrofoil [8]. Overviews of dynamic fault detection as a general field can be found in various sources [9-12]

Although HVAC FDD tends towards steady state analysis, there is an existing literature on dynamic algorithms. Wagner and Shoureshi developed an observer-based scheme for a vapour compression cycle with a fixed orifice device [13]. They model the system with a simplified lumped parameter approach allowing the use of a Kalman filter. Liang and Du produced an FDD method for an air handling unit (AHU) using a lumped parameter model [14]. Parameter estimation is used to update those parameters associated with faulty conditions and a support vector machine is used to diagnose which fault is occurring.

Black box approaches have also been employed in dynamic HVAC FDD. Lee et al. used observer based techniques as well as structured residuals to predict fault in an AHU [15]. Data driven techniques, ARX and ARMAX, were used to model the system behaviour. Physical faults were induced as well as bias in the sensors. Zhou and Dexter took advantage of a fuzzy-relational model to account for nonlinearities in the system [16]. The faults studied were limited to fouling in the heat exchangers.

Keir and Alleyne explored the possibility of using more complex moving-boundary models for FDD in vapour compression cycles [17]. Testing was performed on a subcritical vapour compression cycle. A linearized form of the model was used to explore the sensitivity of each output to a variety of faults; however, no practical FDD algorithm is implemented. This is the only example found in the literature of a sufficiently complex model being used to represent a vapor compression cycle as opposed to an AHU.

Attempts to apply FDD to closed loop systems have also been made. Salsbury and Diamond investigated using feedforward control in conjunction with a PI controller on an AHU [18]. The feedforward controller supplied the normal amount of actuation to reach a set point and any input from the PI controller beyond a certain threshold was taken to be indicative of a fault. Talukdar and Patra synthesized the control and FDD algorithms for an AHU [19].

Steady State Fault Detection

Halm-Owoo and Suen explained many of the steady state methods in use for HVAC FDD [20]. FDD methods were broken into model-based techniques, knowledge-

based methods, and signal processing techniques. Examples were given of a model-based method for detecting fouling in an AHU and of an ANN method for detecting faults in an AHU. Zhou et al. used fuzzy models to identify faulty behaviour in a centrifugal chiller [21]. A neural network was then used to diagnose which fault was occurring. Haves et al. used parameter estimation on a set of nonlinear first-principle functions to detect faults in a system [22]. To eliminate the difficulty of finding parameter values in a nonlinear function an intermediate layer of radial basis functions were used. The analysis was limited to the cooling coil subsystem of an AHU. Tassou and Grace implemented a artificial neural network to identify slow leaks of refrigerant and off-design charge levels in a vapour compression system [23].

Principal Component Analysis (PCA) has become a technique of interest for HVAC FDD. Wang and Cui used a PCA algorithm to find bias in a dozen sensors of a centrifugal chiller system [24]. Chen and Lan used PCA to find fouling of the evaporator or condenser for a heat pump/water chiller in an office building [25]. Li investigated the use of wavelet-PCA and pattern matching-PCA on an AHU [26].

Li and Braun developed a statistical rule based FDD scheme for use in a rooftop air conditioner [27]. Li and Braun later derived a scheme to enable the successful detection of simultaneous faults [28].

More experimental techniques for HVAC FDD have also been employed. Taylor and Corne tested a negative selection algorithm to detect evaporator frosting in a supermarket freezer [29]. An artificial immune system is used to differentiate between normal and faulty behaviour.

The downside of these approaches is the need for large quantities of training data to establish normal operation. Additional faulty data is also necessary if diagnostic capability is desired and absurd amounts of data are required to detect simultaneous faults. Collection of this data is often costly and is specific to a given system. For that reason the work of Li and Braun on component level virtual sensors for FDD is of great interest [30].

Li and Braun also derived a virtual charge sensor based off of simple measurements [31]. Wichman and Braun expanded this approach to FDD on commercial coolers and freezers [32]. Decoupled fault sensors are derived from known physical relationships within the system. This technique has several advantages. It is based off of simple physical relationships within the vapor compression cycle. This limits the need for large amounts of training data. A specific fault indicator is assigned to each common fault and is insensitive to other faults that may occur simultaneously. Because of this, multiple simultaneous faults can be present without affecting accuracy. Li and Braun also derived a method to create virtual pressure measurements from cheaper thermocouples in the system, thereby lowering the cost of sensors [33]. This reduction of cost is an important part of any practical HVAC FDD method. Transferring this method to a transcritical cycle will be the focus of this work due to all these advantages.

THEORETICAL APPROACH

The first aspect of this research was to investigate the use of system dynamics for FDD. The majority of HVAC systems will regularly exhibit steady state or pseudo-steady state behavior at regular intervals during their operation. For example an automotive air conditioner, which will operate in transient during stop and go traffic, will enter steady state while on a freeway. Most residential systems operate with on/off control. By the end of the on cycle they will be very close to steady state conditions. Because both steady state and dynamic FDD are possible for most HVAC systems, focus was given on discovering whether knowledge of dynamic behaviour eases the task of discriminating between faulty and fault-free behaviour.

Dynamic Models

To test this, finite control volume (FCV) models of the transcritical refrigeration cycle were coded and verified with training data. The resulting models were given step inputs with and without simulated faults and the transients were compared. The presence of significant overshoot or change in rise time would indicate a situation in which a dynamic FDD algorithm could theoretically outperform a static algorithm which only has access to the error present at steady state conditions. Figure 2 uses an arbitrary second order transfer function representing an error signal to illustrate the potential gains from a dynamic FDD method. If overshoot is present, a larger error signal is present during transient operation. If no overshoot is present, the dynamic model offers no new information while containing higher computational demands. Additionally a large

change in the rise time can supply information about faulty behavior that is not available at steady state.

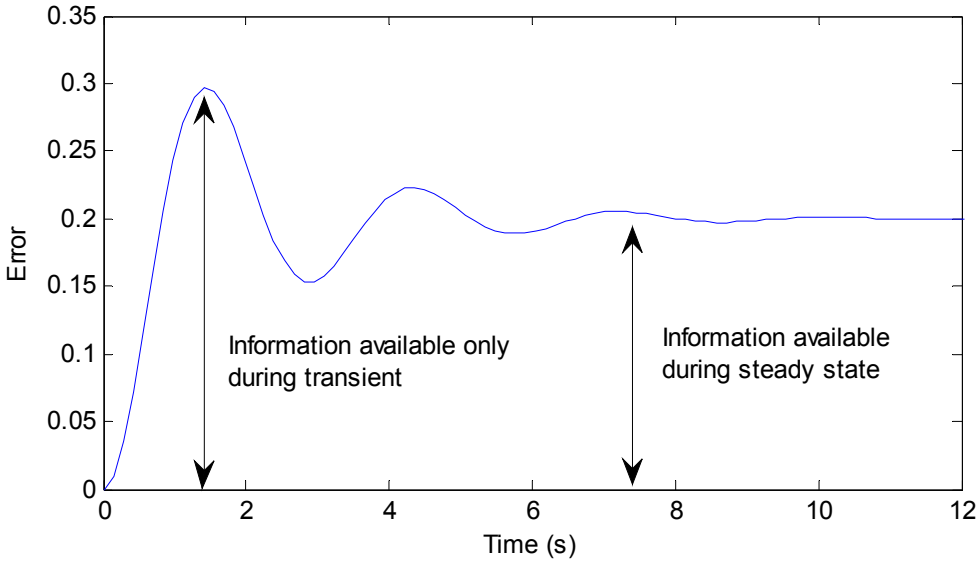

Figure 2. Example of the value of dynamic FDD

The dynamic models of the transcritical vapour compression cycle were made in Simulink using modified versions of models coded for subcritical system. In these models, each component is treated as an independent subsystem, linked to one another by inputs and outputs. These components are the evaporator, the gas cooler, the electronic expansion valve (EEV), and the compressor. Figure 3 shows the complete FCV model within Simulink. The following paragraphs will briefly detail some of the assumptions used in the derivations of these models.

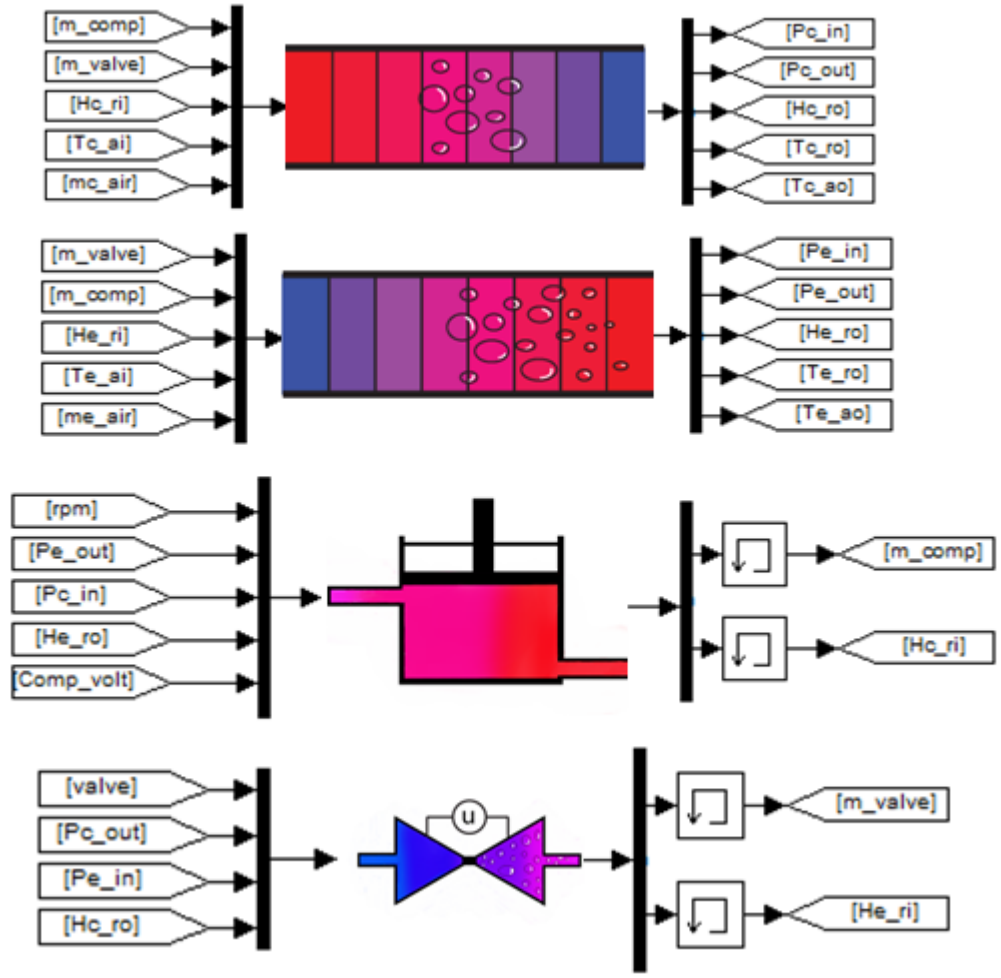

Figure 3. FCV model in Simulink

The FCV models of the evaporator and gas cooler are first made by treating the heat exchanger as one long tube. The geometry and features such as fins are not directly accounted for; however, their effects can be approximated by modifying the effective parameters of heat exchanger. The fluid flow is treated as one dimensional. In reality there is often turbulent flow present. A good selection of heat transfer coefficient will mask this.

An assumption is made that there is little variation of refrigerant properties along the radial axis. This assumption is valid as the heat transfer coefficient between the refrigerant and the tube wall is much lower than that within the refrigerant. Additionally, the tube wall is too thin to contain a large temperature differential in the radial direction.

The final assumption regards the pressure drop within the heat exchanger due to viscous friction in the fluid flow. This is treated as negligible leaving each heat exchanger with constant pressure along its length. The omission of this calculation greatly simplifies the construction of the model as well as improves run time.

The heat exchanger is broken up into n control volumes during the modelling process. Each control volume is deemed to have uniform refrigerant properties, uniform wall temperatures, and uniform heat transfer coefficients. The states of the equation are the refrigerant enthalpy at each node, the wall temperature at each node, and the overall pressure of the heat exchanger. This gives a total of $2n+1$ dynamic states. Figure 4 shows a diagram of the FCV heat exchanger.

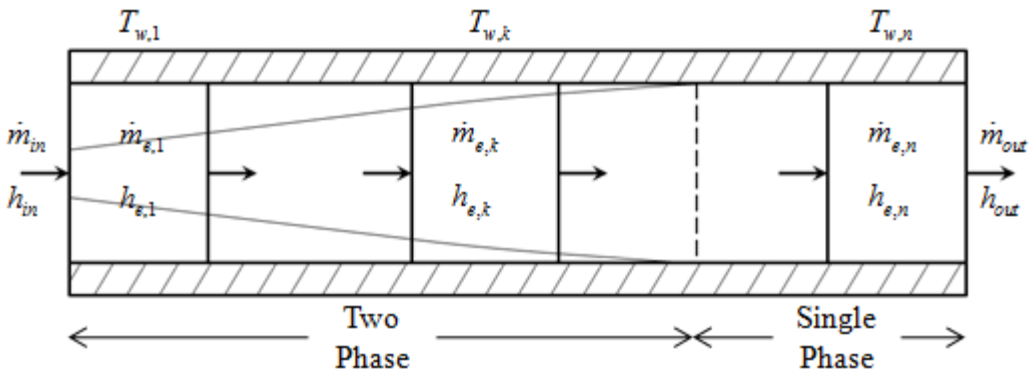

Figure 4. FCV heat exchanger model

The derivation of the models springs from the conservation of energy and mass equations. The conservation of energy is applied twice at each node. The change in the refrigerant enthalpy within the node must be equal to total energy leaving the refrigerant to the wall added to any energy change from a difference in the inlet and outlet mass flow rates for the node. An energy balance is also applied between to the tube wall at each node. The change in the wall temperature must be equal to the difference in the energy moved inside the tube from the refrigerant and the energy moved outside the tube from the flow of air over the heat exchanger. Finally, a mass balance is substituted at each node to remove the intermediate mass flow terms. Eq. 1 shows the three conservation equations together in vector form. Eq. 2 through 4 give the structure for the heat exchanger models. Details of the model and its derivation can be found in the appendix.

$$\begin{bmatrix} \dot{U}_1 \\ \vdots \\ \dot{U}_k \\ \vdots \\ \dot{U}_n \\ \dot{m}_{hx} \\ \dot{E}_{w,1} \\ \vdots \\ \dot{E}_{w,k} \\ \vdots \\ \dot{E}_{w,n} \end{bmatrix} = \begin{bmatrix} \dot{m}_{in}h_{in} - \dot{m}_1 h_1 + \alpha_{i,1}A_i(T_{w,1} - T_{r,1}) \\ \vdots \\ \dot{m}_{k-1}h_{k-1} - \dot{m}_k h_k + \alpha_{i,k}A_i(T_{w,k} - T_{r,k}) \\ \vdots \\ \dot{m}_{n-1}h_{n-1} - \dot{m}_n h_n + \alpha_{i,n}A_i(T_{w,n} - T_{r,n}) \\ \dot{m}_{in} - \dot{m}_{out} \\ \alpha_{o,1}A_o(T_{a,1} - T_{w,1}) - \alpha_{i,1}A_i(T_{w,1} - T_{r,1}) \\ \vdots \\ \alpha_{o,k}A_o(T_{a,k} - T_{w,k}) - \alpha_{i,k}A_i(T_{w,k} - T_{r,k}) \\ \vdots \\ \alpha_{o,n}A_o(T_{a,n} - T_{w,n}) - \alpha_{i,n}A_i(T_{w,n} - T_{r,n}) \end{bmatrix} \tag{1}$$

$$Z(x,u)\dot{x} = f(x,u) \tag{2}$$

$$x = \begin{bmatrix} P & h_1 & \dots & h_k & \dots & h_n & T_{w,1} & \dots & T_{w,k} & \dots & T_{w,n} \end{bmatrix}^T \tag{3}$$

$$u = \begin{bmatrix} \dot{m}_{in} & \dot{m}_{out} & h_{in} & T_{air,in} & \dot{m}_{air} \end{bmatrix}^T \tag{4}$$

The equations governing the evaporator and gas cooler are identical in their derivation. Differences do arise when the models are implemented. For example there is no two-phase region inside of the gas cooler. It is a single-phase supercritical fluid for the entire length. The other primary difference is in the internal heat transfer coefficients. In each node at each time step the convective heat transfer coefficient must be calculated for both the internal surface and external surface of the heat exchanger.

Two sets of correlations are used in the evaporator. The correlation of Thome and Hajal is used to calculate the internal coefficient in the two-phase regions [34]. It is a version of the general evaporative heat transfer correlation derived by Kattan et al. adapted specifically for carbon dioxide [35]. For the region which contains pure vapor, a correlation by Gnielinski for general vapor flow in heat exchangers [36]. For the gas cooler only one heat transfer correlation was required, that of Yoon et al. for use in supercritical cooling of carbon dioxide [37]. The equations governing these heat transfer coefficients are present in the Appendix.

Because the dynamics are much faster than those of the evaporator or gas cooler, the dynamics of the valve and compressor are ignored. Instead they are represented with static algebraic equations. The EEV is modelled with the orifice equation, seen in Eq. 5.

$$\dot{m}_v = C_d A_v \sqrt{\rho_e (P_{gc} - P_e)} \tag{5}$$

C_d is the coefficient of discharge, $\dot{m}_v$ is the mass flow rate of the valve, A_v is the area of the valve opening, P_{gc} is the pressure of the gas cooler, P_e is the pressure of the evaporator, and ρ_e is the fluid density at the valve inlet.

The coefficient of discharge is an empirical quantity that is dependent on the geometry of the valve as well as the fluid properties. The area of the valve opening is also not directly known, but is dependent on the input signal to the EEV. Assuming a linear relationship over a small range, this equation can be rewritten into Eq. 6.

$$\dot{m}_v = (v_1 + v_2 u_{valve}) \sqrt{\rho_e (P_{gc} - P_e)} \tag{6}$$

Here v_1 and v_2 are empirical coefficients, and u_{valve} is the command sent to the EEV. Details of how to calculate v_1 and v_2 without a mass flow meter are explained by Hariharan [38].

The model for the compressor is taken from previous work by Rasmussen and Alleyne [39]. Eq. 7 shows the algebraic formula used.

$$\dot{m}_c = \rho_c \left[k_1 - k_2 \left(\frac{P_{gc}}{P_{evap}} \right)^{1/n} \right] \tag{7}$$

Here $\dot{m}_c$ is the mass flow rate of the compressor, ρ_c is the density of the refrigerant at the compressor inlet, and k_1, k_2 and n are empirical parameters found in the same manner as those for the EEV.

Static Fault Relationships

The goal of these relationships is to derive for the most common faults physical relationships within the vapour compression cycle that are responsive to one particular fault while being independent of all other faults. Ideally, this should also be done while using a minimum of sensors and avoiding costly measurements such as mass flow or pressure. The majority of these relationships are versions of those found in Wichman and Braun modified to work for a transcritical cycle [32].

Gas Cooler and Evaporator Fouling

Fouling occurs when debris blocks air flow over either of the heat exchangers on a HVAC system. The first sensor for detecting fouling on the evaporator or gas cooler is based off a simple energy balance. At steady state operation the amount of energy

leaving the refrigerant must equal that entering the air flow. This relationship can be solved to obtain the mass flow rate of air over the heat exchanger as in Eqs. 8 and 9.

$$\dot{m}_{gca,est} = \frac{\dot{m}_{comp}(h_{gcri} - h_{gcro})}{c_{p,a}(T_{gcao} - T_{gcai})} \tag{8}$$

$$\dot{m}_{ea,est} = \frac{\dot{m}_{comp}(h_{eo} - h_{ei})}{c_{p,a}(T_{eai} - T_{eao})} \tag{9}$$

For Eq. 8, $\dot{m}_{gca,est}$ is the estimated mass flow rate of air over the gas cooler, $\dot{m}_{comp}$ is the mass flow rate of the refrigerant as determined from the manufacturer's compressor map, h_{gcri} is the refrigerant gas cooler inlet enthalpy, h_{gcro} is the refrigerant gas cooler outlet enthalpy, $c_{p,a}$ is the specific heat of air, T_{gcao} is the gas cooler inlet air temperature, and T_{gcai} is the gas cooler outlet air temperature. For Eq. 9, $\dot{m}_{ea,est}$ is the estimated mass flow rate of air over the evaporator, h_{eri} is the refrigerant evaporator inlet enthalpy, h_{ero} is the refrigerant evaporator outlet enthalpy, T_{eao} is the evaporator inlet air temperature, and T_{eai} is the evaporator outlet air temperature.

Undercharge and Overcharge

The next faults under consideration were undercharge and overcharge of refrigerant. Wichman and Braun suggest using the difference between superheat and subcooling to find this fault in the form of Eq. 10 [32].

$$\Delta T_{sh-sc} = k_{sc,sh}(T_{sh} - T_{sh,nom}) - (T_{sc} - T_{sc,nom}) \tag{10}$$

ΔT_{sh-sc} is the fault indicator, $k_{sc,sh}$ is an empirical constant designed to remove sensitivity to inlet air temperatures, T_{sh} is the measured superheat, $T_{sh,nom}$ is the normal superheat of the system, T_{sc} is the measured subcooling, and $T_{sc,nom}$ is the normal subcooling of the system. Superheat is defined as the difference between the evaporator exit temperature and the saturation temperature for the refrigerant at that pressure. It is typically used to ensure that no liquid is entering the compressor. Subcooling is the difference between the saturation temperature in the condenser and the condenser outlet temperature. Unfortunately, a transcritical system lacks subcooling as refrigerant in the gas cooler is a supercritical fluid and never becomes a liquid.

For that reason an alternative approach was used. A correlation can be made with the refrigerant densities at the entrance and exit of each heat exchanger and the overall system charge. The densities can be calculated given the pressure and temperature measurements at each location Eq. 11 shows the resulting formula.

$$\Delta C = \rho_{eri} + \alpha_1 \rho_{ero} + \alpha_2 \rho_{gcri} + \alpha_3 \rho_{gcro} \tag{11}$$

ΔC is the fault indicator, ρ_{eri} is the evaporator inlet density, ρ_{ero} is the evaporator outlet density, ρ_{gcri} is the gas cooler inlet density, ρ_{gcro} is the gas cooler outlet density, and α_1, α_2, and α_3 are empirical coefficients. Training data for the coefficients only occurs at the nominal charge condition which simplifies the process of commissioning the system.

Compressor Valve Leakage

The final fault to be tested was the compressor valve leakage. This leads to a reduction in the volumetric efficiency of the compressor causing a drop in the

compressor outlet temperature. Wichman and Braun suggested creating a virtual sensor for compressor outlet enthalpy [32]. Eq. 12 shows this formula.

$$h_{kro,est} = h_{ero} + \frac{\dot{W}_{comp} - \dot{Q}_{loss}}{\dot{m}_{comp}} \tag{12}$$

Here $h_{kro,est}$ is the compressor exit enthalpy to be estimated, $\dot{W}_{comp}$ is the compressor work as determined from a manufacturer's map, and $\dot{Q}_{loss}$ is the heat loss of the compressor which is found empirically.

The formula Wichman and Braun recommend for $\dot{Q}_{loss}$ is based off and approximation of the compressor shell temperature [32]. However, this works poorly for a transcritical system due to a much higher compressor outlet temperature. For that reason a correlation for $\dot{Q}_{loss}$ was made using the measured difference in inlet and exit enthalpy as displayed in Eq. 13.

$$\dot{Q}_{loss} = \left[\beta_1 + \beta_2 (h_{kro} - h_{ero})\right] \dot{W}_{comp} \tag{13}$$

β_1 and β_2 are empirically derived coefficients, which can be calculated from the same set of training data as those for the virtual mass sensor.

The fault indicator for the compressor valve leakage is given by Eq. 14.

$$\Delta T_{kro} = T_{kro,est} - T_{kro} \tag{14}$$

ΔT_{kro} is the fault indicator, $T_{kro,est}$ is derived from P_{gc} and $h_{kro,est}$, and T_{kro} is the measured compressor outlet temperature [38].

EXPERIMENTAL APPARATUS

The experimental transcritical system, seen in Figure 5, is built using a donated drinks cabinet, such as would be found in a grocery or convenient store.

Figure 5. Experimental transcritical CO2 system

The system is a basic vapor compression cycle without any receiver, accumulator, or internal heat exchanger. It consists of an electronic expansion valve (EEV), a compressor, a gas cooler and an evaporator. A bypass valve was later added to simulate

the compressor valve leakage fault; however, it is normally kept closed. Eight thermocouples have been installed. Four are placed within the lines to measure the refrigerant temperature between each component. The other four are placed before and after the heat exchangers on the air side to calculate inlet and outlet temperatures. Pressure sensors are located on the high and low side. Only two are installed as pressure drops in the heat exchangers are assumed to be negligible. The overall layout is given by Figure 6.

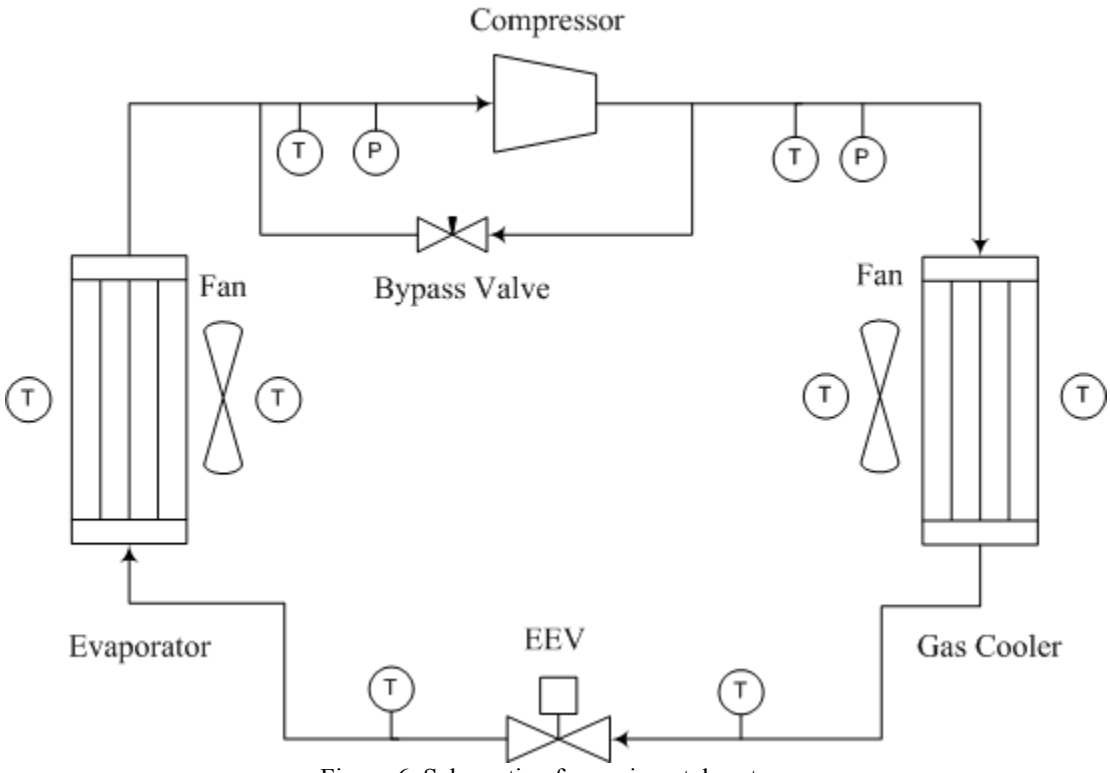

Figure 6. Schematic of experimental system

All piping connecting system components is ¼in stainless steel with Swagelok compression fittings. Additionally, two safety features have been added to prevent injury in the case of high discharge pressure. A pressure relief valve set to activate should the compressor outlet pressure rise above 13 MPa was added. Also a pressure switch was added which opens the compressor circuit if the pressure rises above 11.2 MPa. Neither has any effect on normal system operation.

The compressor is a TN-1410 prototype from Danfoss. It is a fixed-speed reciprocating compressor powered by a 240 V signal at 50 Hz. Because of the high discharge temperature, external cooling is supplied by the gas cooler fan. The compressor provides approximately 0.5 kW of cooling while operating under normal conditions. Figure 7 shows the TN-1410 compressor.

The gas cooler and the evaporator are both tube and fin type heat exchangers. The external fluid, air, moves over in cross flow. The fans that provide this flow are variable voltage allowing for user control. For the evaporator there is 10.8m of ¼in copper tubing in twenty-four passes with 124 external fins. The gas cooler has 16.3m of tubing in forty-four passes with 62 external fins. The gas cooler can be seen in Figure 8.

Figure 7. The compressor

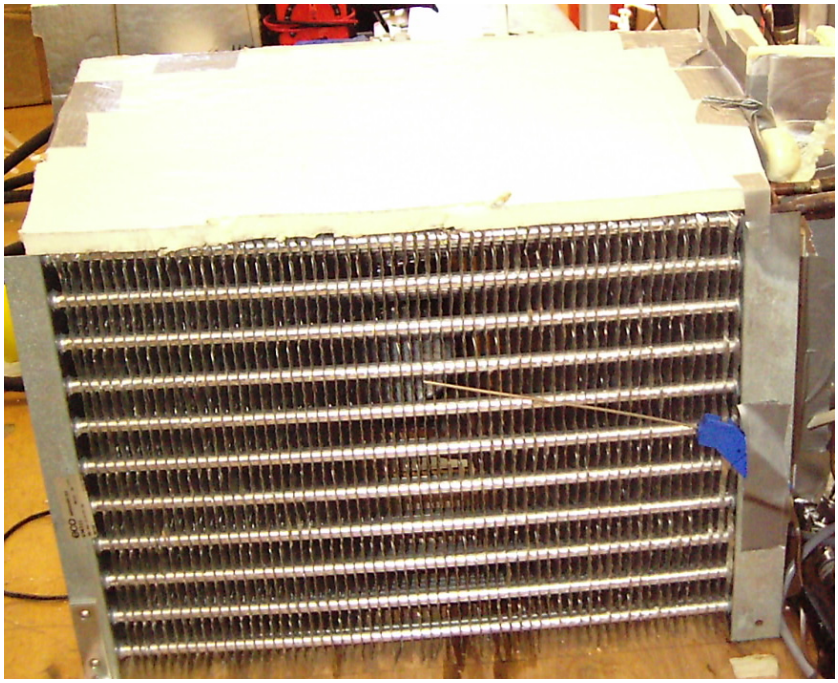

Figure 8. The gas cooler

The EEV is a prototype UKV-J14D donated to the lab by Danfoss-Saginomiya. It is capable of providing cooling between 0.25 kW and 10 kW. The UKV-A111 coil adjusts the opening of the valve. Control of the EEV is accomplished by the LNE-ZP30 board which in turn accepts a 0-10 V signal. A view of the EEV without its external fittings is shown in Figure 9.

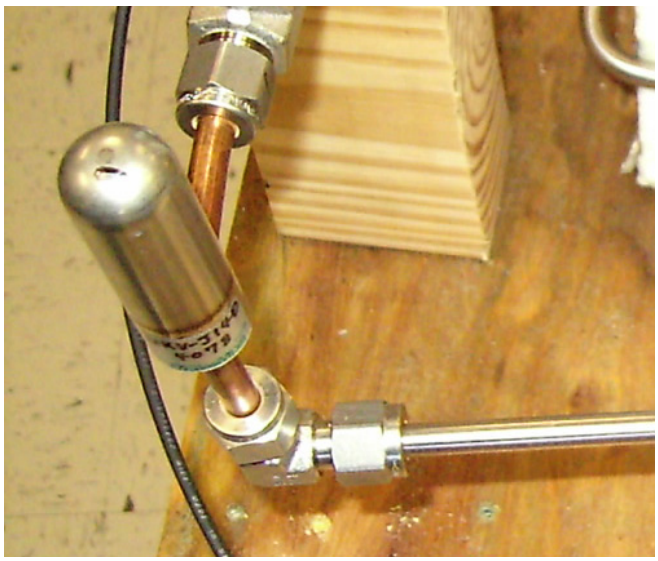

Figure 9. The UKV-J14D EEV

The system's bypass valve is the SS-4GUF4-G needle valve from Swagelok. In the shut position it seals completely allowing no flow. This allows the system to operate normally when the compressor valve leakage fault is not being simulated. Control of the valve is accomplished via a manually operated handle. Figure 10 shows the bypass valve connected across the compressor.

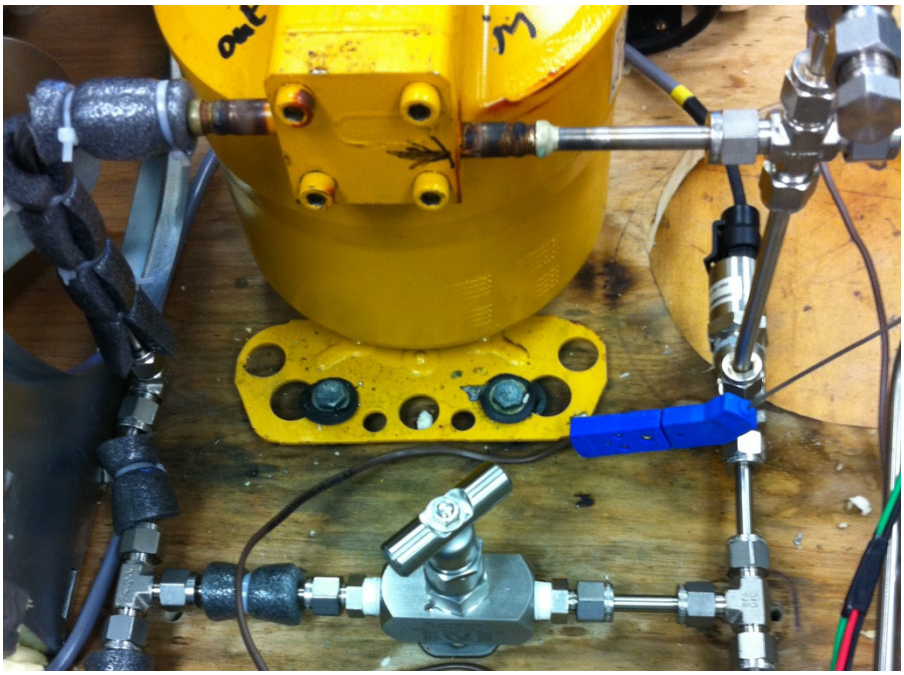

Figure 10. The bypass valve attached to the compressor

Figure 11. Fan speed control boards

The fans for the evaporator and the gas cooler are controlled by independent boards from Controls Resources. They accept an input signal from the data acquisition computer. Figure 11 shows the control boards for each fan

Temperature measurements are conducted with GJMQSS-125G-6 T-type thermocouples from Omega. They are used to measure both refrigerant and air temperatures. The thermocouples are accurate to ±0.5°C. Processing of the data is done by a Measurement Computing PCI-DAS-TC thermocouple board. One of the thermocouples is displayed in Figure 12.

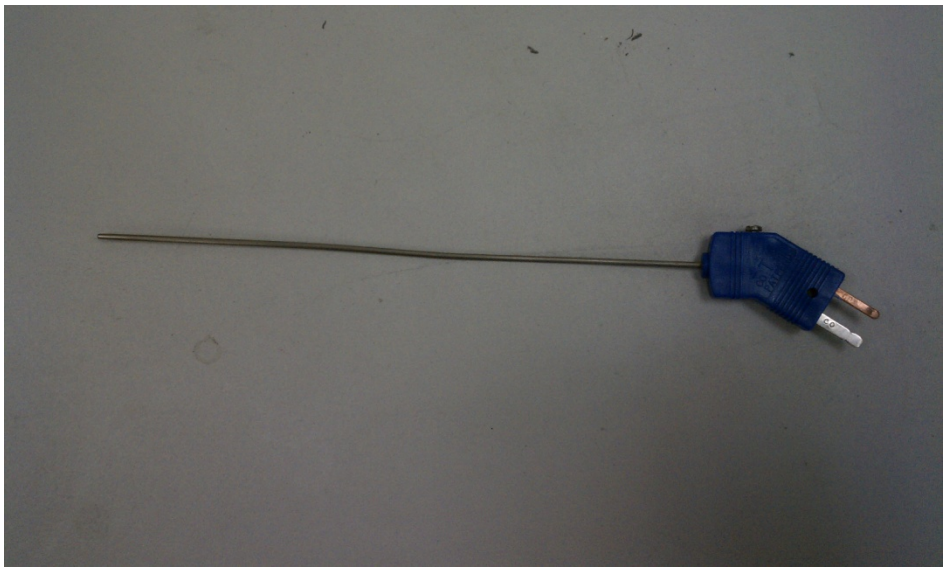

Figure 12. Type-T thermocouple

The system pressures are measured using 84HP piezoresistive pressure sensors from Sensata. They are capable of measuring pressures up to 17 MPa and are accurate to ±45kPa. Figure 13 shows one of the pressure sensors attached to piping.

Figure 13. Pressure sensor

Table 2. Parts list for transcritical refrigeration system

Part	Manufacturer	Part No.	Quantity
EEV	Danfoss Saginomiya	UKV-J14D (Prototype)	1
EEV Motor	Danfoss Saginomiya	UKV-A111	1
EEV Control Board	Danfoss Saginomiya	LNE-ZP30-110	1
Compressor	Danfoss	TN-1410 (Prototype)	1
Evaporator	Unknown	N/A	1
Gas Cooler	Unknown	N/A	1
Fan	General Electric	5KSM81HFL3012S	2
Fan Controller	Control Resources	180V800E	2
Bypass Valve	Swagelok	SS-4GUF4-G	1
Thermocouple	Omega	GJMQSS-125G-6	8
Pressure Sensor	Sensata	84HP062X02500SS0C	2
High Pressure Cutoff Switch	Sensata	PS80-21-XXXX	1

A list of all major components can be seen in Table 2. Control of the system is achieved with a data acquisition PC. Various sensor modules from Dataforth allow the reading and output of electrical signals. Wincon is the software used to operate the system. It allows Simulink to be the user interface for the system. Figure 14 shows the data acquisition computer while Figure 15 shows the software interface.

Figure 14. The DAQ PC

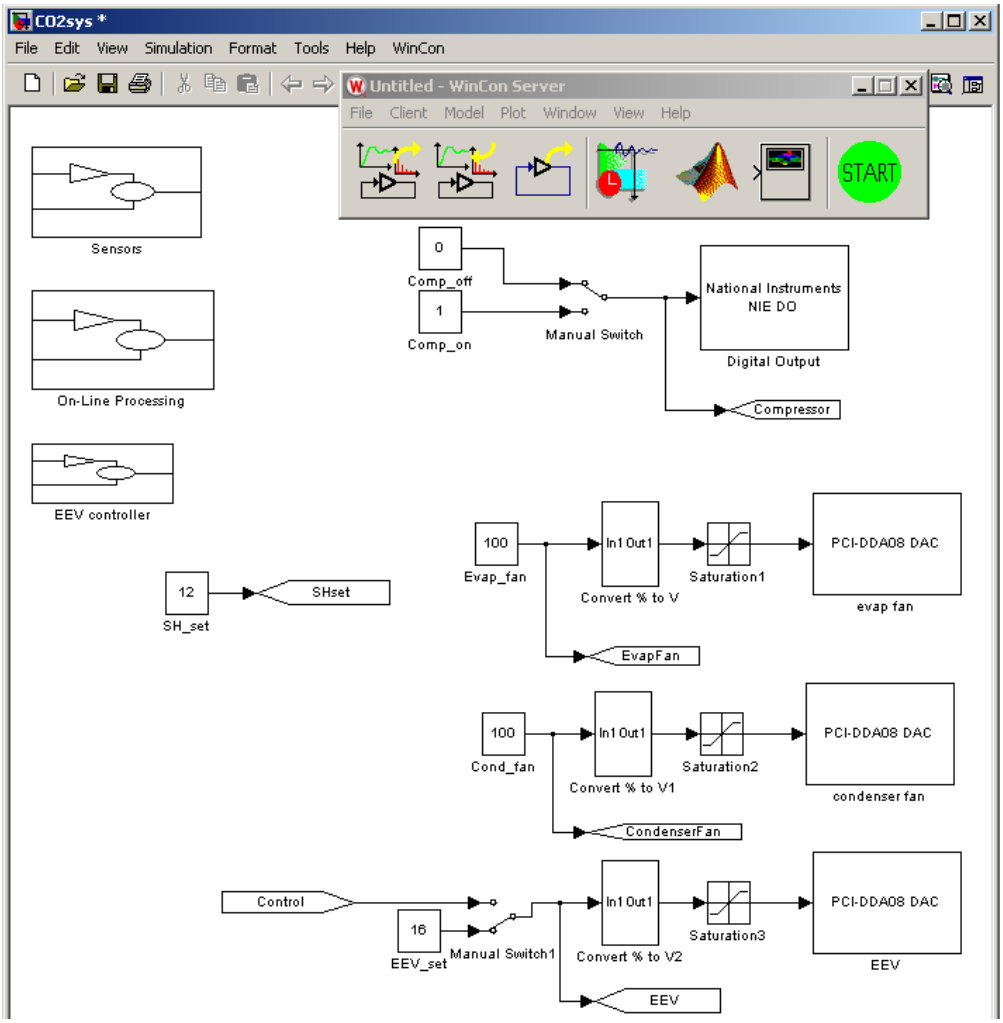

Figure 15. Wincon and Simulink interface

Subcritical System

The subcritical system selected for comparison was a TRANE residential air-conditioning unit currently used in the Thermofluids Controls Lab. It provides three tons of cooling and has actuation in the valve, both fans, and two-speed control in the condenser. The refrigerant used is R-410a. Other than the instrumentation, this unit would be equivalent to a high end home unit. Figure 16 is a picture of the TRANE system and Figure 17 depicts the layout.

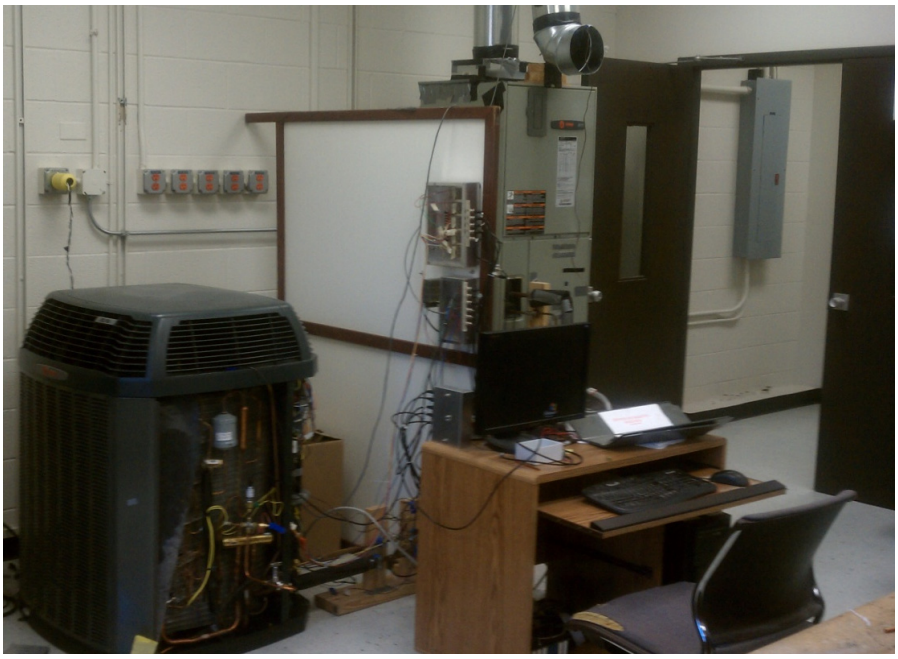

Figure 16. The TRANE subcritical air conditioner

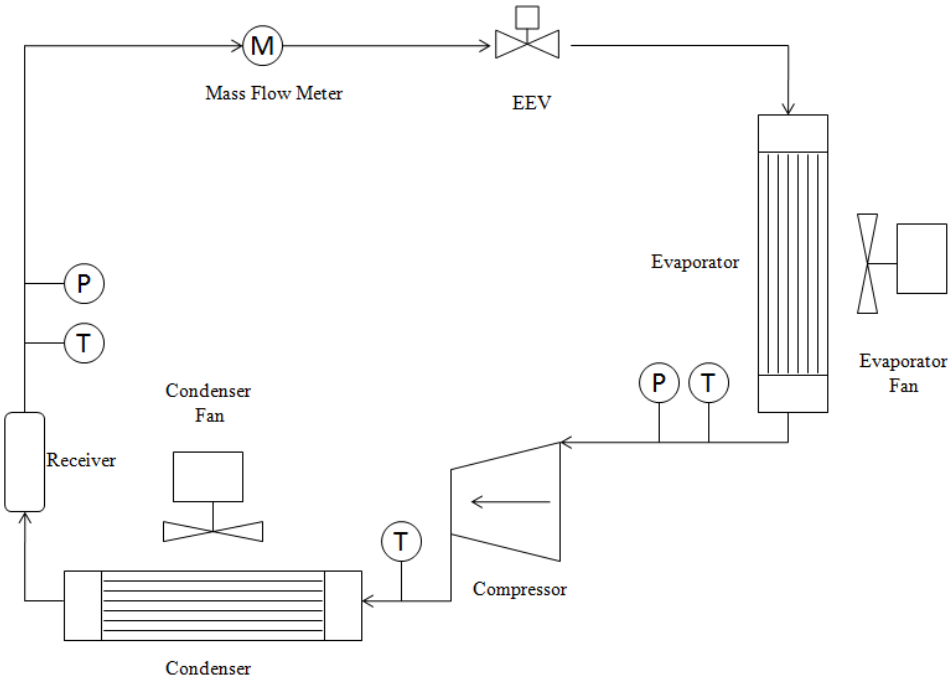

Figure 17. Schematic of the system's layout

DYNAMIC FAULT DETECTION

To test the potential efficacy of dynamic fault detection it is necessary to see whether any overshoot is present in the step responses of the transcritical system or whether its responses or primarily first order. A first order response means that the maximum change in an error signal would occur at steady state. This means that the error signal would not be larger during transients. Because modeling the dynamics in a vapor compression system is much harder than deriving a static model, a first order response would reflect poorly on the practicality of any dynamic fault detection method.

Dynamic Responses for Transcritical System

Step tests were performed on the system for the valve, the gas cooler fan, and the evaporator fan to provide insight to normal system behavior. Because of the inherent nonlinearities within the system, these responses would be slightly different if taken at other operating conditions; however, they are indicative of typical responses.

Transcritical Step Responses

The results of these steps in the system pressures as well as the superheat will be given. A Butterworth filter has been used to reduce noise from the data. Figure 18 shows the response to a step decrease in the evaporator fan for the suction pressure, discharge pressure, and superheat.

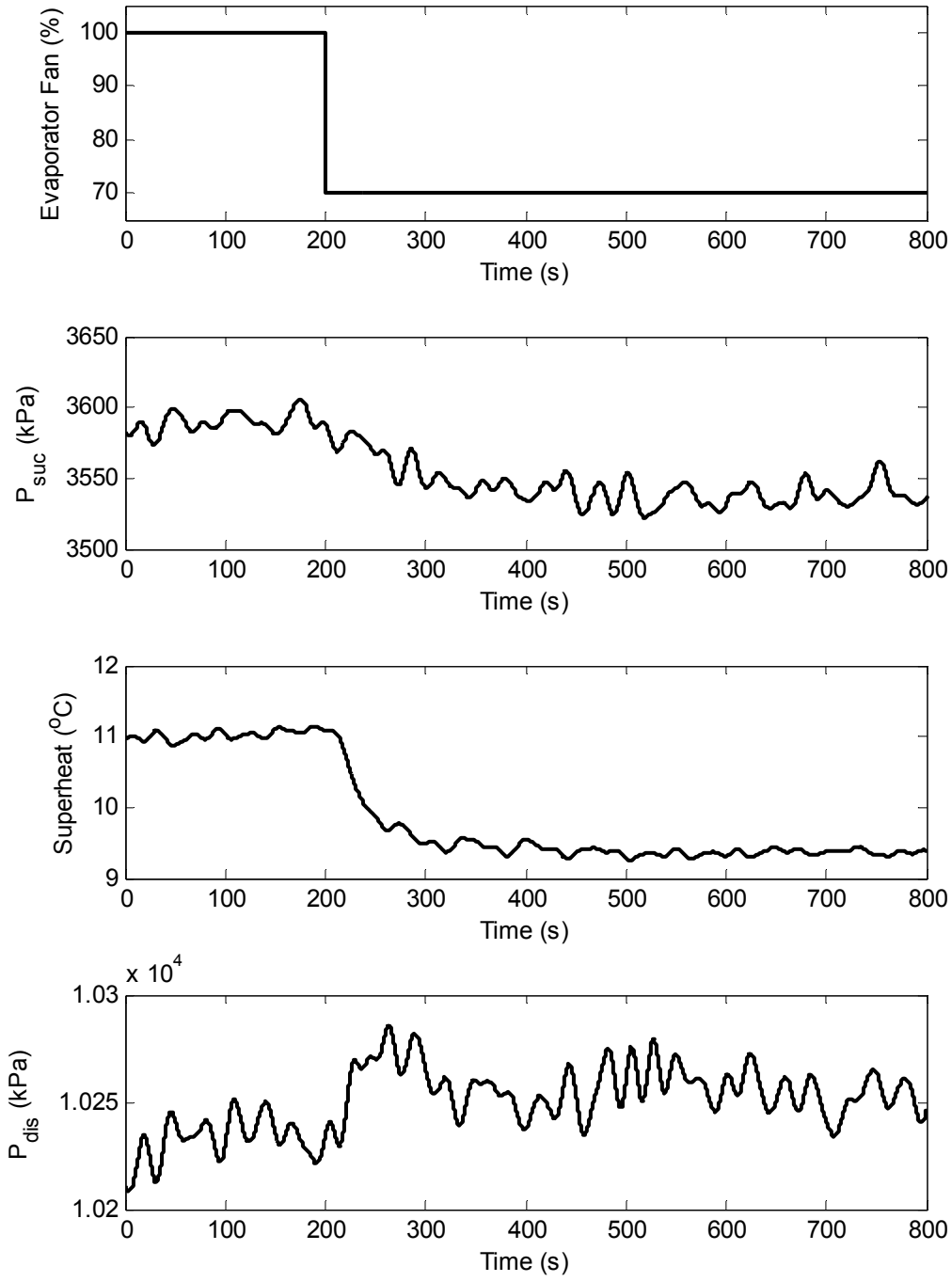

Figure 18. Response to step input in evaporator fan under fault-free conditions

No overshoot is present in any of these responses making it unlikely that any beneficial information could be added with a dynamic fault detection method over a static one. There is also a great deal of noise present in the pressure measurements which makes the exact shape of the step response hard to discern. Figure 19 shows the reaction of the same variables to a step increase in the valve's position.

In the response to the valve there is some minor overshoot present. This overshoot is confined to the response of the superheat and is only a small fraction of the size of the overall step. Figure 20 shows the response to a step decrease in the gas cooler fan for evaporator pressure, gas cooler pressure and superheat.

For steps in the gas cooler fan there is little response in the evaporator pressure or superheat. The gas cooler pressure has a large response due to a drop in cooling in the gas cooler; however, Figure 20 shows that there is no overshoot present.

Transcritical Dynamic Error Signals

Because an enormous combination of faults and output variables exist, the FCV model of the transcritical refrigeration cycle was used to select the most promising combinations for actual testing. Simulations were performed identifying three combinations of a fault, a step to an input, and a response variable that contained the most overshoot in the error signal.

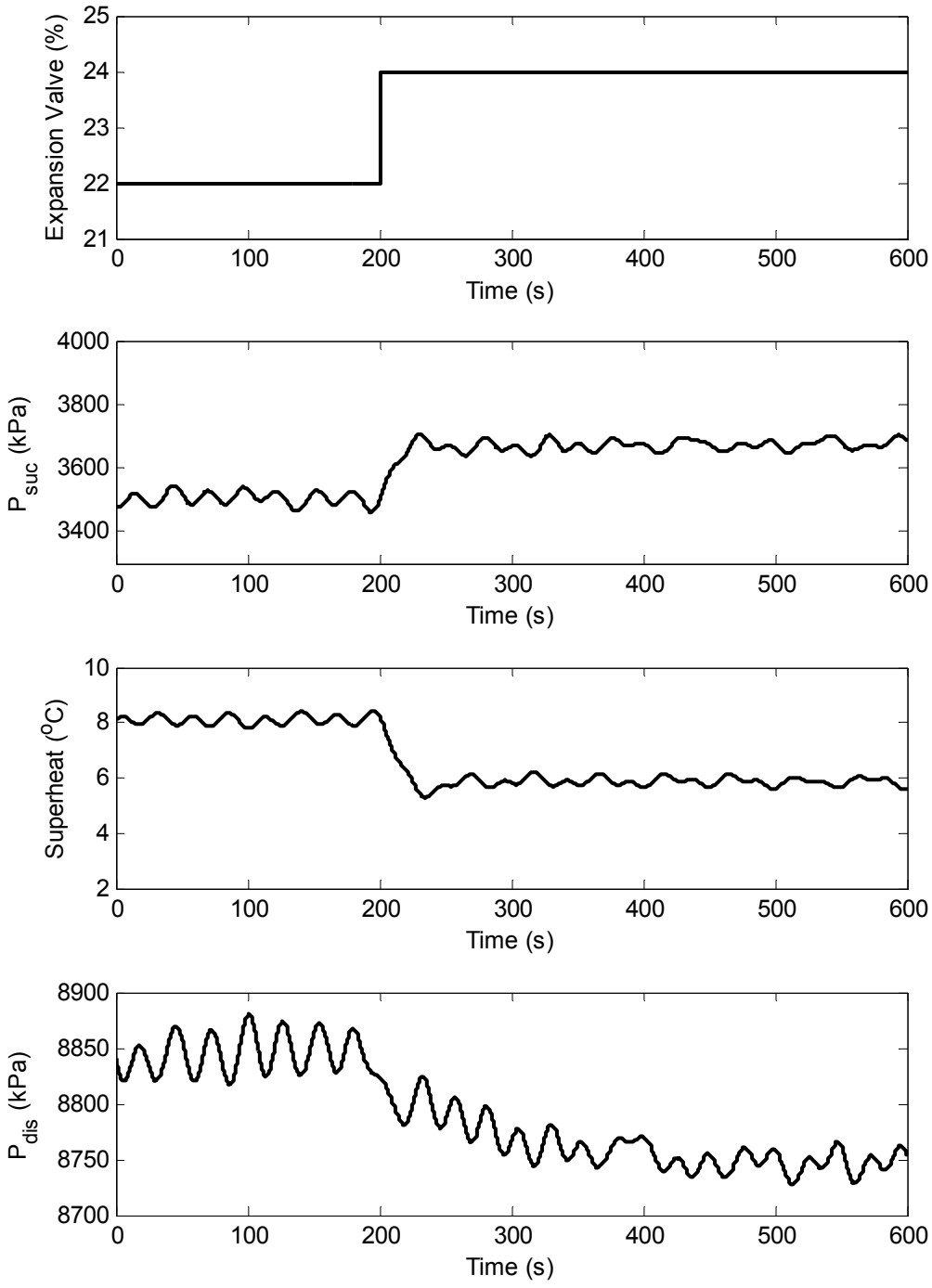

Figure 19. Response to step input in the valve under fault free conditions

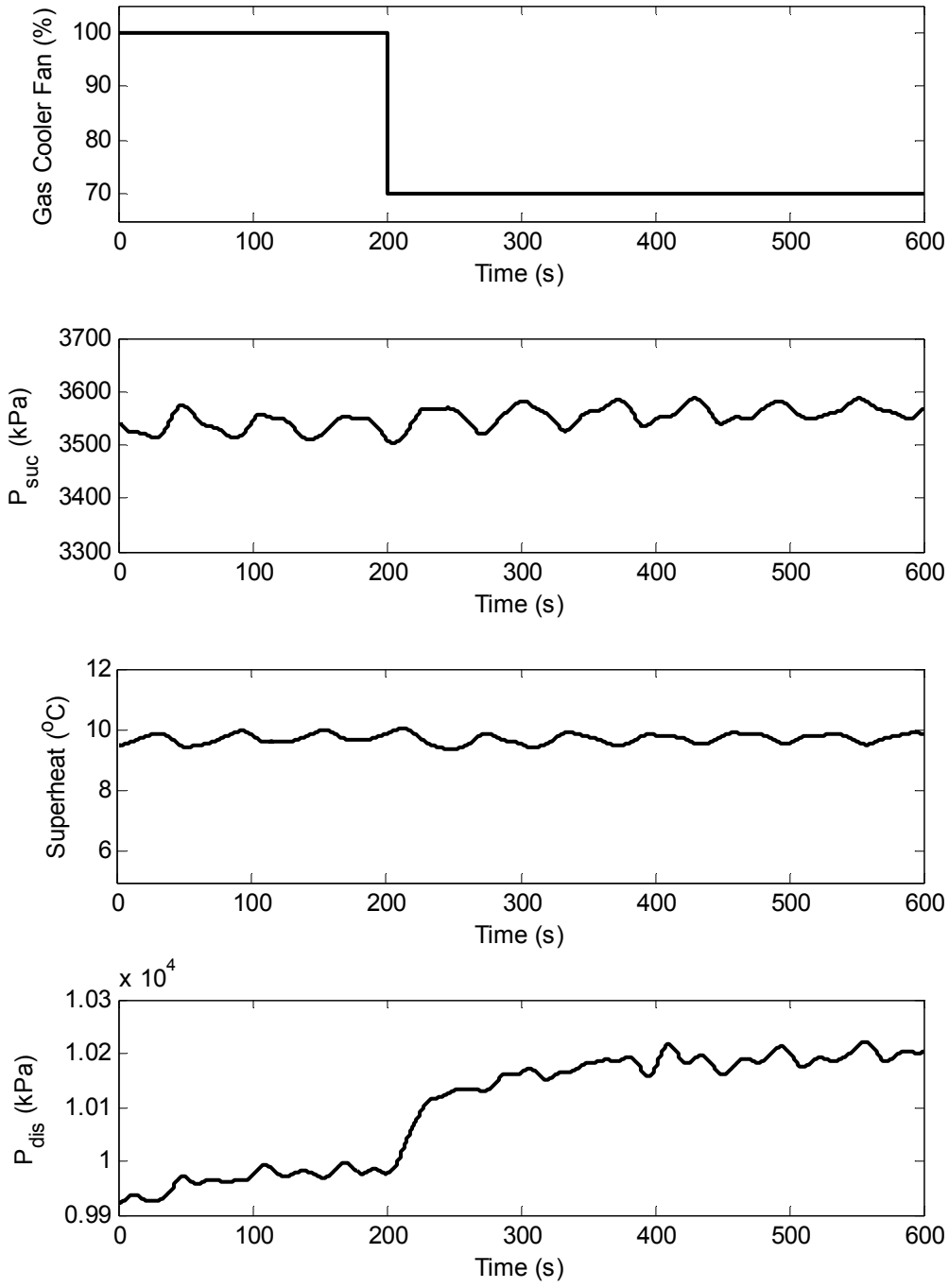

Figure 20. Response to step input in the gas cooler fan under fault-free conditions

The error signal in this case was defined as the absolute value of the difference between the normal response to a step input and the faulty response. Eq. 15 defines the error signal.

$$E(t) = \left| x_{normal}(t) - x_{faulty}(t) \right| \tag{15}$$

Here $E(t)$ is the error signal, $x_{normal}(t)$ is the normal response, and $x_{faulty}(t)$ is the faulty response. Table 3 gives the three best candidates for dynamic fault detection.

Table 3. Candidates for dynamic fault testing

Fault	Step Input	Output	Steady State Error	Overshoot
Evaporator Fouling	Evaporator Fan	P_{dis}	39 kPa	8 kPa
Gas Cooler Fouling	Valve	P_{dis}	690 kPa	2 kPa
Undercharge	Valve	P_{dis}	700 kPa	15 kPa

All three combinations of faults and inputs have the gas cooler pressure as the variable in which overshoot is expected to occur. Table 3 clearly shows that only trivial amounts of overshoot can be expected in the error signals. No combination has enough overshoot to exceed the accuracy of the sensors. Nonetheless testing for each of these combinations was performed. As a note, the steady state error for the faults will not perfectly match the model as the faults induced during testing were not the same size and not at identical operation points.

For evaporator fouling a decrease in the evaporator fan was selected as the most promising step input. To simulate the fault a blockage was put in front of the evaporator fan. The step input was a 30% decrease in the evaporator fan input voltage which corresponds to a 15% decrease in the mass flow rate of air over the evaporator. No overshoot was detected in the error signal as well as no major changes in rise time. Figure 21 shows the error signal for this test. As with the previous section, time is normalized such that all steps occur at 200 seconds.

In the presence of gas cooler fouling a step in the valve position was deemed most likely to induce overshoot in the gas cooler pressure. To simulate gas cooler fouling the input voltage to the gas cooler fan was decreased by 30% corresponding to a 20% reduction in the mass flow rate of air over the gas cooler. The step was a 2% opening of the valve. Figure 22 shows the error signal in the gas cooler pressure for this step test. If any overshoot is present, noise in the system makes it undetectable. Also no noticeable change in the rise time occurs.

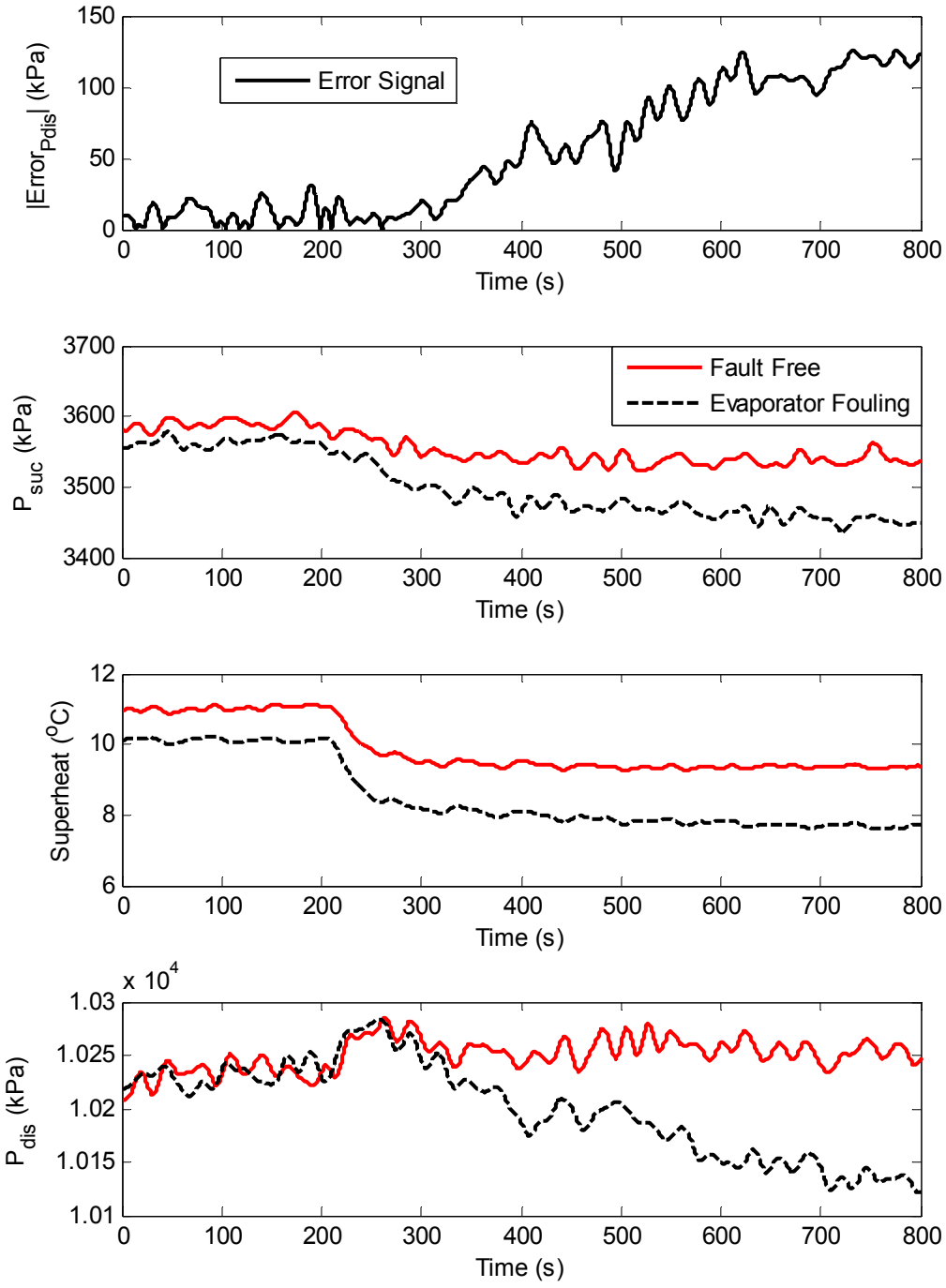

Figure 21. Error in system to an evaporator fan step with evaporator fouling

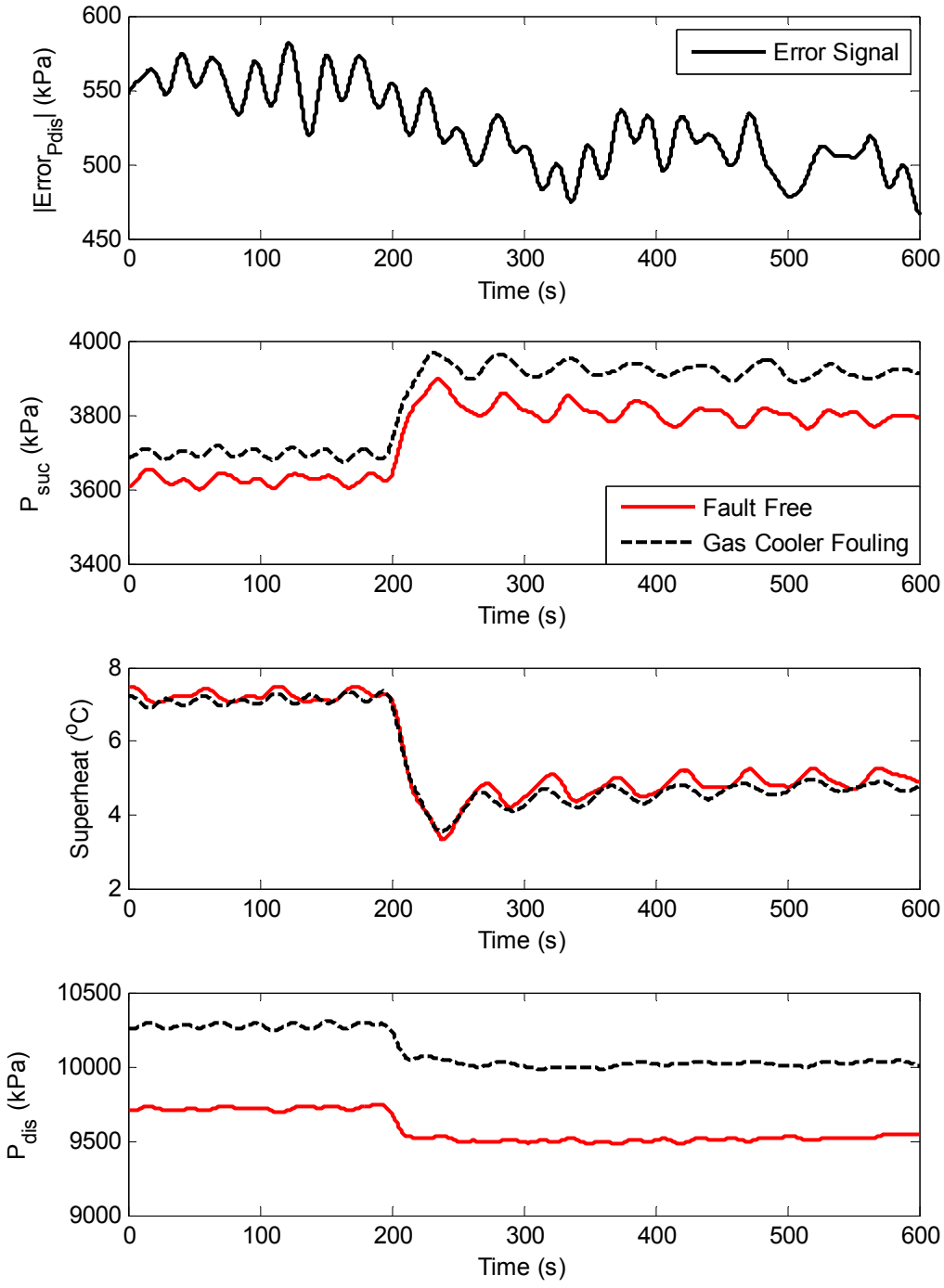

Figure 22. Error in system to a valve step with gas cooler fouling

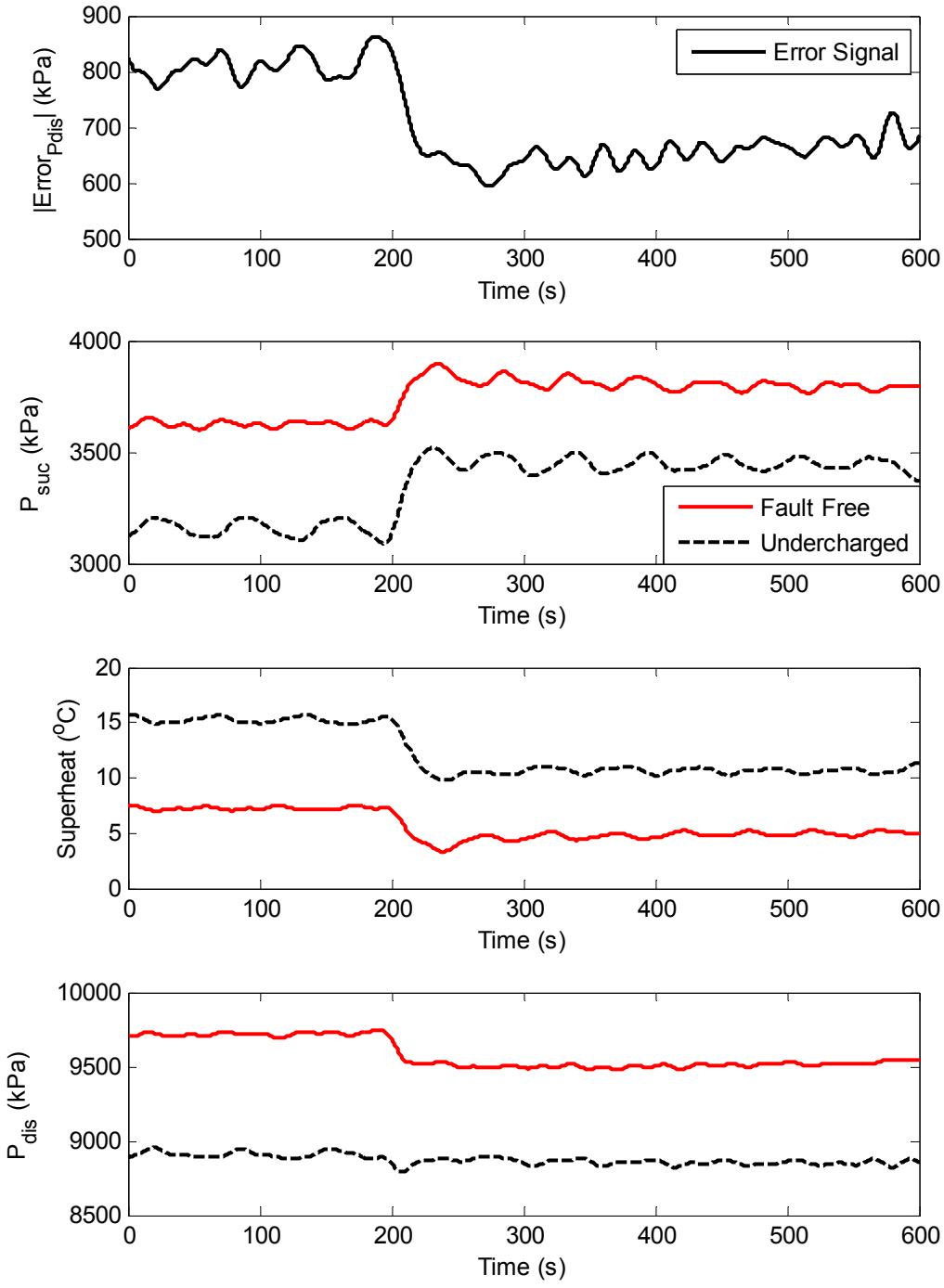

Figure 23. Error in system to valve step while undercharged

When the transcritical system is undercharged, the valve step was deemed most likely to induce overshoot. To simulate the fault the system was charged 85% of its normal charge level. The valve opening was given a 2% step increase. Figure 23 gives the error signal in the gas cooler pressure for this test. A small amount of overshoot is present; however, when it is compared with the steady state magnitude of the error signal it is trivial. No significant changes in rise time are seen.

For the tested transcritical system there do not seem to be any faults or inputs that will cause large amounts of overshoot. First order responses tend to dominate. In the few cases where overshoot is present, it is extremely minor. For this reason it is unlikely that the use of dynamic fault detection could offer much benefit over static methods and nearly impossible that it would justify the increased complexity of modelling dynamic system behavior.

Comparison to Subcritical Dynamics

To render the results more general the same combinations of faulty conditions and step inputs were performed on the subcritical system. The undercharge condition was dropped, though, due to the presence of a receiver which minimizes the effect of deviations in charge. This comparison is not meant to exhaustively test the viability of dynamic fault detection in subcritical systems. It is merely meant to be used to help evaluate the findings presented on transcritical dynamic fault detection.

Subcritical Step Responses

To begin step tests were given to each actuator as was done with the transcritical system. The results of these steps on the condenser pressure, evaporator pressure, and superheat will be given. The first step was given to the evaporator fan. Figure 24 shows the responses in evaporator pressure, condenser pressure, and superheat. None of the responses contain any detectable amount of superheat. First order responses predominate.

For the next step test, a step was given to the expansion valve and the results were recorded. Figure 25 gives the step responses for the evaporator pressure, condenser pressure, and superheat. There is clearly no overshoot present in the condenser pressure or superheat. A very small amount is visible in the evaporator response; however, relative to noise and measurement errors it is insignificant.

The final step test under normal conditions was given to the condenser fan. Figure 26 shows the reaction of the subcritical air-conditioning system to a sudden change in condenser fan speed. No overshoot is present in the suction pressure or in the discharge pressure despite a large change in the latter. A small amount can be seen in the superheat; however, it is only about 0.5°C. None of the step responses to evaporator fan, valve, or condenser fan show great promise in terms of dynamic fault detection.

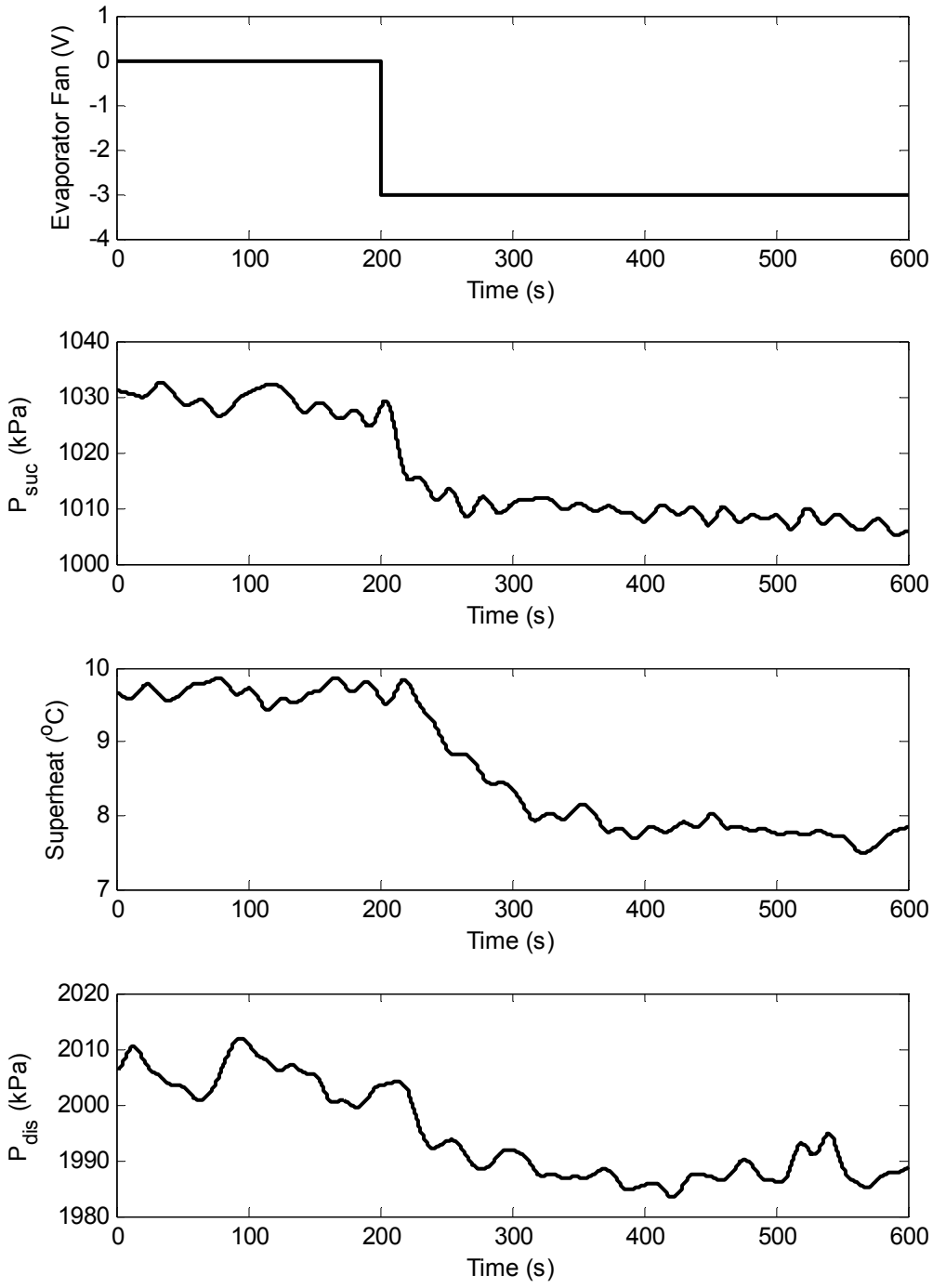

Figure 24. Subcritical response to a step in the evaporator fan under fault-free conditions

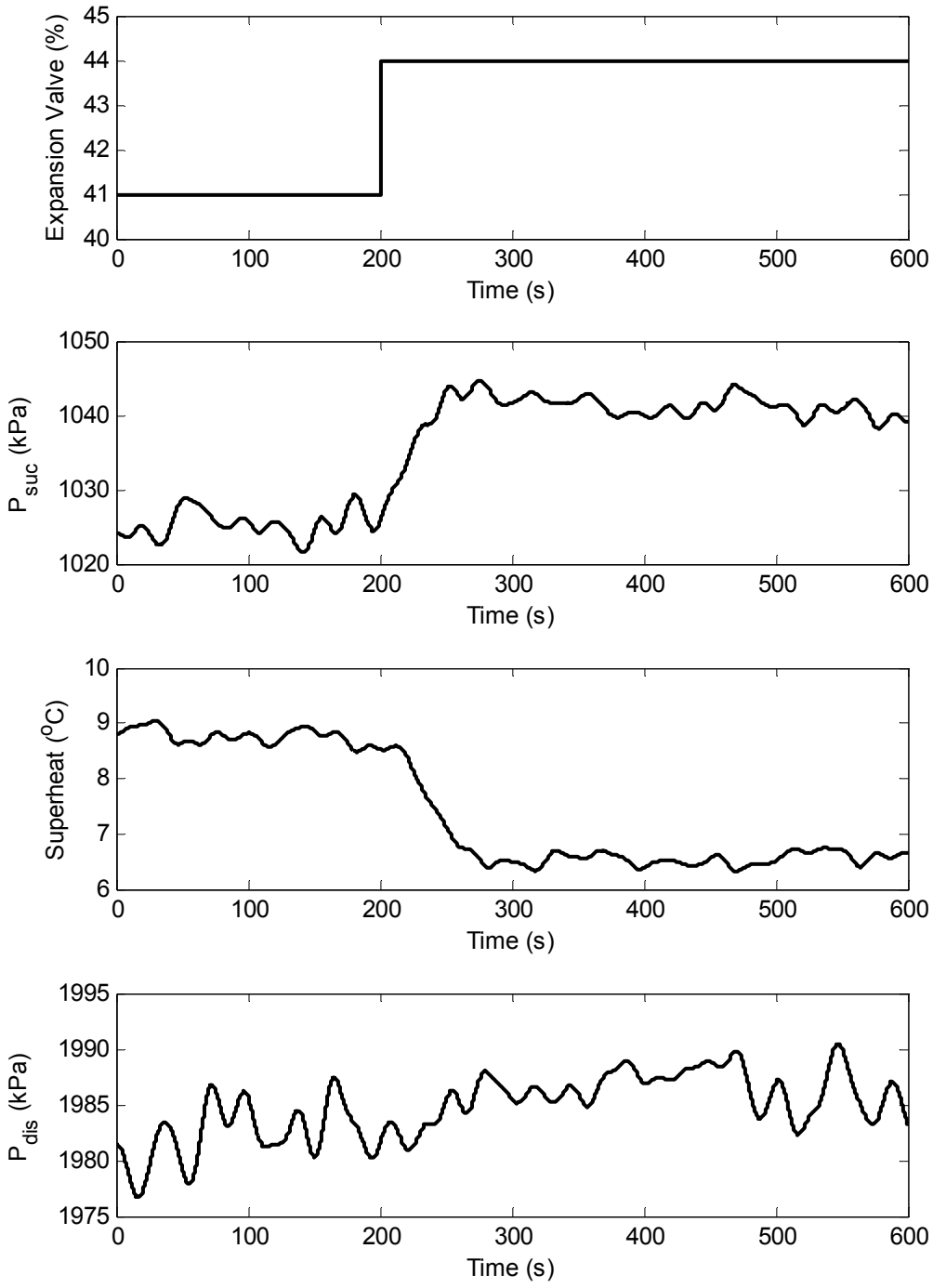

Figure 25. Subcritical response to a step in the valve under fault-free conditions

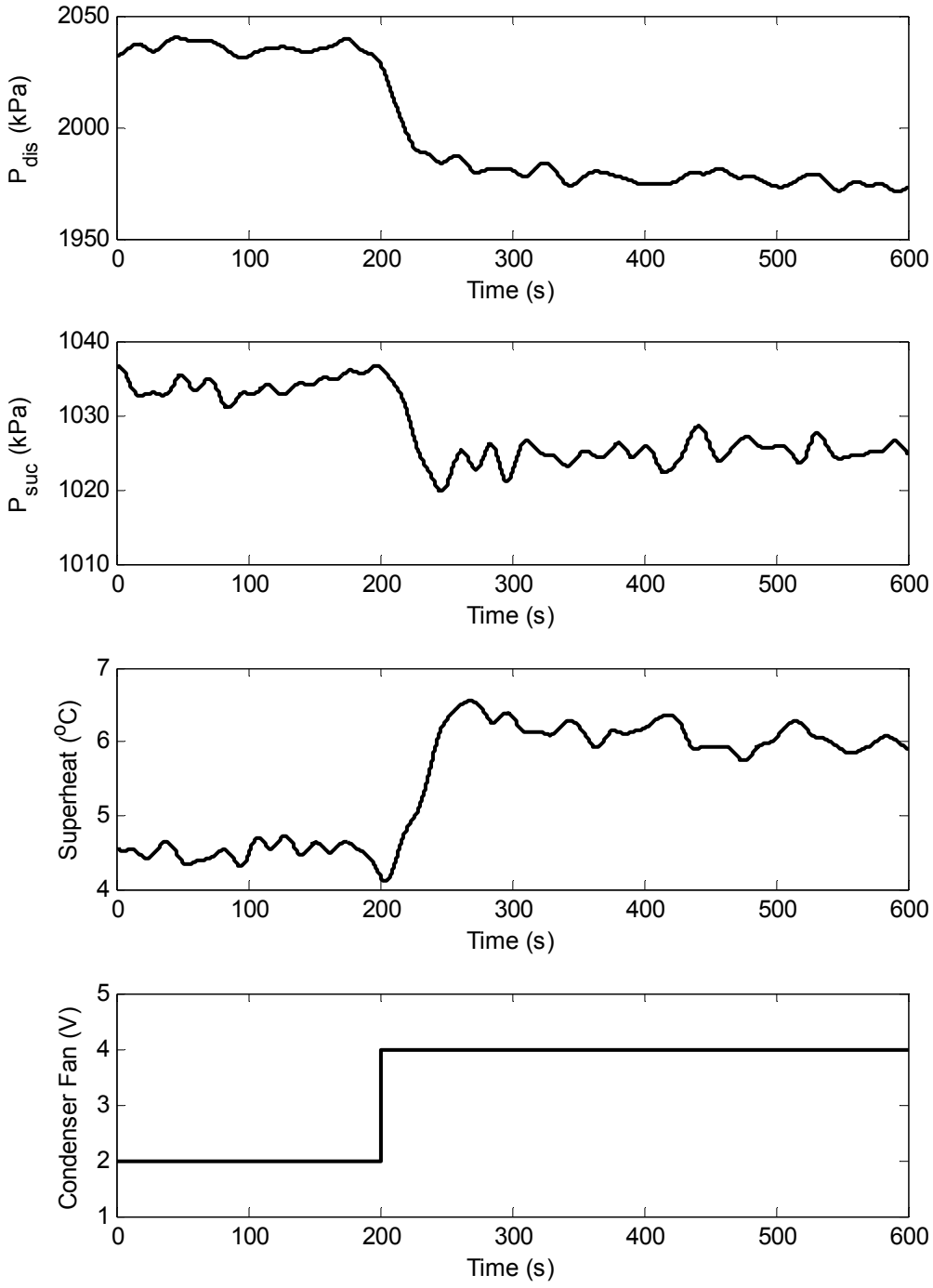

Figure 26. Subcritical response to a step in the condenser fan under fault-free conditions

Subcritical Dynamic Error Signals

The tests to find overshoot in the error signals for the transcritical system were also replicated for the subcritical system. First the effects of evaporator fouling were tested. To simulate the fouling a blockage was placed over part of the evaporator air inlet. A step was given to the evaporator fan equivalent to approximately a 20% reduction in evaporator mass flow. The difference of the step test for faulty and fault-free conditions was taken, and the error for the condenser pressure appears in Figure 27. There is little change in the error and no overshoot is present. No change in rise time is visible.

The other fault simulated was condenser fouling. To simulate that the condenser fan input voltage was lower until the air flow had been reduced by approximately 25%. The valve was opened by 3% to induce dynamics. Figure 28 shows the error in the condenser pressure signal as the test was conducted. No overshoot is found.

As with the transcritical dynamic tests no real amounts of overshoot were found during any of the scenarios tested. The static errors in signals dwarf any additional information that may be gained from including dynamics. This adds support to the notion that there is no value in incorporating dynamic analysis into HVAC fault detection and diagnosis.

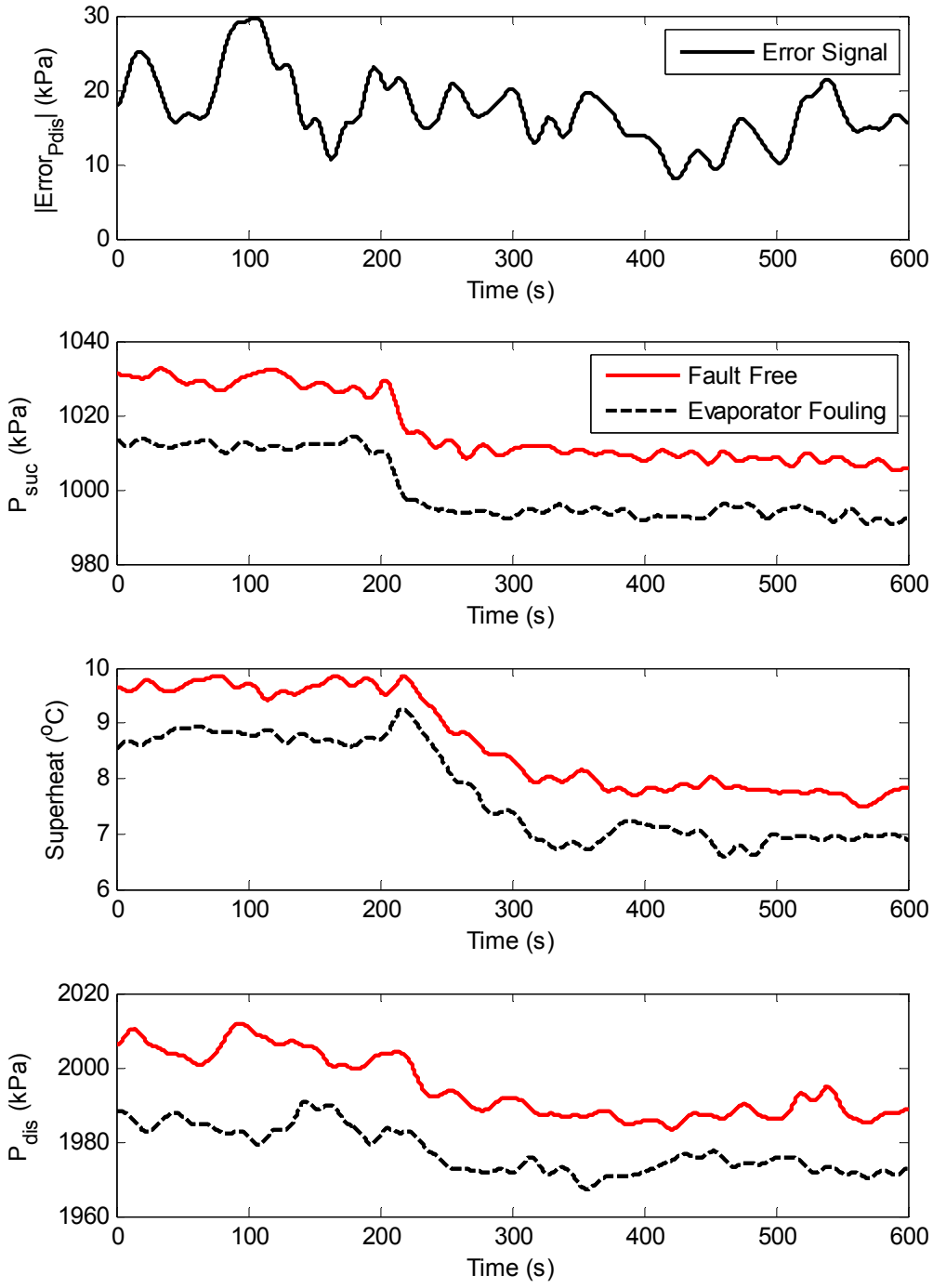

Figure 27. Error in system to evaporator fan step with evaporator fouling present

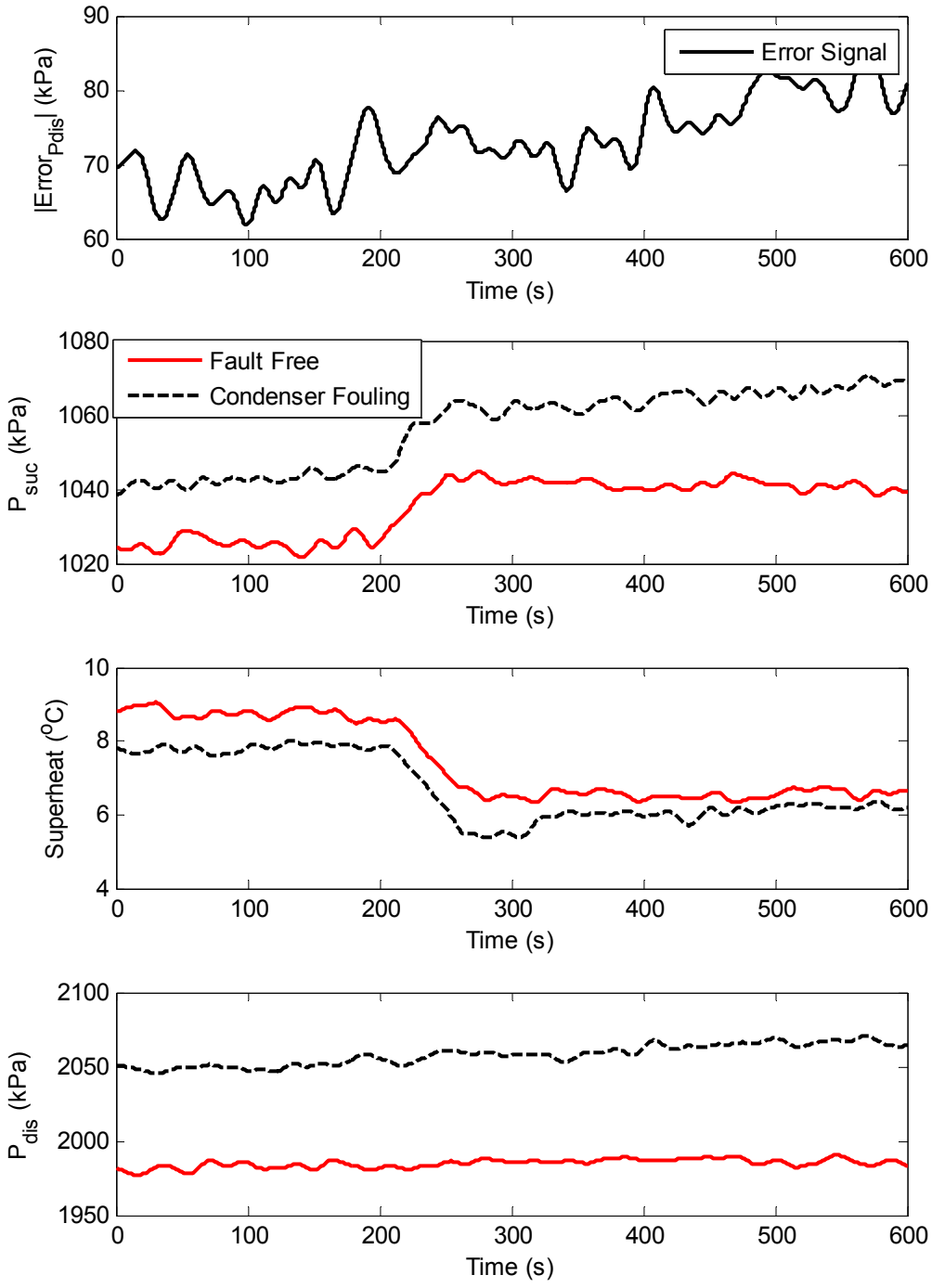

Figure 28. Error in system to valve step with condenser fouling present

STATIC FAULT DETECTION

Testing for the static fault detection method was performed in one continuous test. This was done to reduce any opportunities for confounding factors to appear. All faults were tested individually as well as in binary pairs. The transcritical system was completely drained of all carbon dioxide using a vacuum pump. It was then filled to low-charge condition and testing was initiated. Table 4 shows the order of the fault detection test.

Table 4. Test order for static fault detection

Order	Fault 1	Fault 2
1	Undercharge	None
2	Undercharge	Gas Cooler Fouling (Air Flow)
3	Undercharge	Evaporator Fouling (Air Flow)
4	Undercharge	Compressor Valve (Air Flow)
5	None	None
6	Gas Cooler Fouling (Air Flow)	None
7	Gas Cooler Fouling (Air Flow)	Evaporator Fouling (Air Flow)
8	Evaporator Fouling (Air Flow)	None
9	Evaporator Fouling (Physical Blockage)	None
10	Gas Cooler Fouling (Physical Blockage)	None
11	Compressor Valve	None
12	Compressor Valve	Gas Cooler Fouling (Air Flow)
13	Compressor Valve	Evaporator Fouling (Air Flow)
14	Overcharge	Gas Cooler Fouling (Air Flow)
15	Overcharge	None
16	Overcharge	Evaporator Fouling (Air Flow)
17	Overcharge	Compressor Valve

The system was allowed to run for approximately twenty minutes in each configuration to achieve steady state operation. There was also a section of data used for training some of the fault indicators that occurred in between configurations four and five. This consisted of eight data points created with changes in the EEV, evaporator fan, and gas cooler fan. Later this data was used to determine the empirical coefficients in the virtual sensors for charge level and compressor valve leakage. Table 5 gives the values for the fault indicators during the test.

Table 5. Fault indicators for each test

Faults		Indicator			
Fault 1	Fault 2	Charge	Gas Cooler Air Flow (kg/min)	Evaporator Air Flow (kg/min)	ΔT_{ko} (°C)
Undercharge	None	-36.1	6.4	4.9	0.4
Undercharge	Gas Cooler Fouling	-36.1	4.6	4.7	1.1
Undercharge	Evaporator Fouling	-33.9	7.0	3.2	-0.1
Undercharge	Compressor Valve	-19.9	7.1	5.2	4.7
None	None	-2.7	7.5	4.2	1.2
Gas Cooler Fouling	None	-1.0	5.0	4.0	0.8
Gas Cooler Fouling	Evaporator Fouling	-5.5	5.4	2.6	-0.1
Evaporator Fouling	None	-4.8	8.8	2.1	0.4
Evaporator Fouling (P)	None	-3.4	7.9	3.7	1.0
Gas Cooler Fouling (P)	None	-0.4	5.3	4.0	0.9
Compressor Valve	None	2.3	8.2	4.5	2.3
Compressor Valve	Gas Cooler Fouling	2.2	5.9	4.7	2.2
Compressor Valve	Evaporator Fouling	-2.1	11.6	3.4	1.2
Overcharge	Gas Cooler Fouling	13.4	4.6	3.7	-0.7
Overcharge	None	12.4	6.8	3.9	-0.5
Overcharge	Evaporator Fouling	5.6	6.2	2.2	-0.9
Overcharge	Compressor Valve	18.0	8.6	4.5	3.3

During the test for combined undercharge and compressor valve leakage, the system underwent a brief period of unstable behavior. After this the system returned to a second different equilibrium point. This behavior has been seen before during the construction and testing of this system. As of now the cause of this is not confirmed. Possible explanations include contaminants in the refrigerant, flaws in some of the prototype equipment, or multiple equilibria in a transcritical system as suggested by Mehta and Eisenhower [40]. The results of the fault indicators at that point have been excluded from the rest of the data and will be presented separately in Table 6.

The charge indicator was the only sensor that continued to function correctly. Both gas cooler and evaporator airflow were significantly overestimated, even though air flow was at the normal speed. Additionally, the compressor exit temperature was accurately predicted by the sensor for compressor valve leakage even though it should not have been given that the compressor valve leakage fault was present.

Table 6. Fault indicators for secondary equilibrium

Fault	Units	Indicator
Charge	None	-43.0
Gas Cooler Air Flow	kg/min	12.4
Evaporator Air Flow	kg/min	11.0
ΔT_{ko}	°C	-0.2

Transcritical Results

In order to get a better assessment of the potential for false positives during operation, a secondary test was also run. In it the system was run at the borders of its operating region for both high and low superheat conditions. To do this the system was tested with both high and low fan speeds for each fan. In the resulting data the transients were removed and the standard deviation of each indicator was taken. In all of the following graphs the points three standard deviations from the normal operating condition will be marked. Any points outside of this window show behavior that is statistically significant ($p<0.01$) either in terms of indicating a fault or showing some cross coupling between sensors. Table 7 shows the standard deviations of each fault indicator. The values three standard deviations from the fault-free point and the point with no secondary fault will be shown on the figures.

Table 7. Standard deviation of fault indicators for system operating region

Indicator	σ (68%)	3σ (99.7%)
Charge	2.78	8.34
Gas Cooler Fouling	0.102	0.306
Evaporator Fouling	0.174	0.522
Compressor Valve	0.7	2.1

Virtual Pressure Measurements

To reduce costs the evaporator pressure sensor can theoretically be replaced by a thermocouple measuring the temperature of the two-phase refrigerant as it enters the

evaporator. Figure 29 compares the results of the two measurements. The results are very close to the measurement error of the interpolated pressure of 50kPa caused by errors in the thermocouple readings of ±0.5°C.

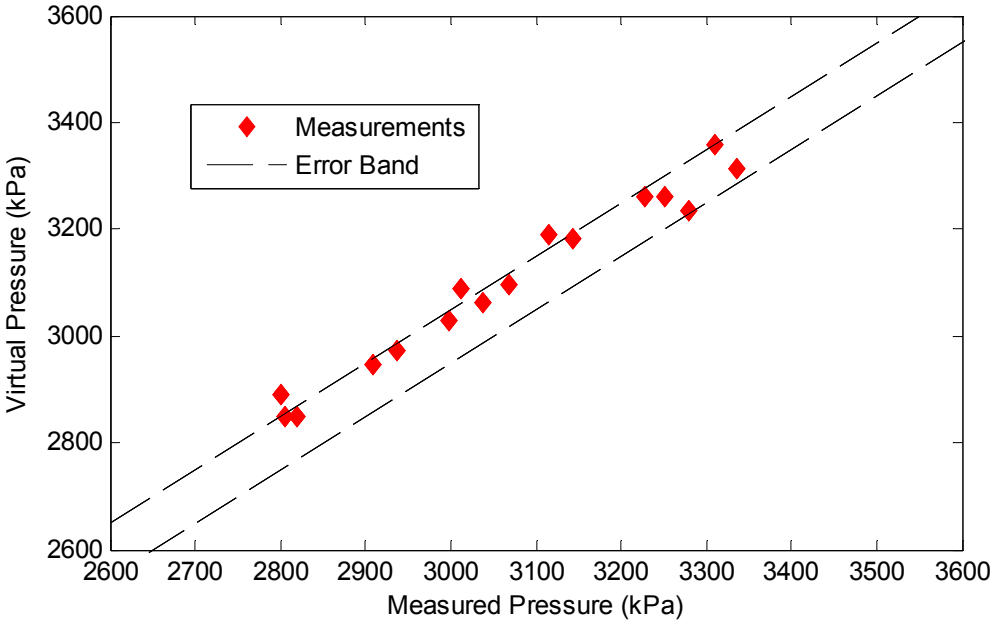

Figure 29. Virtual sensor for pressure measurements

Overcharge and Undercharge

For the undercharged configuration a deviation of -15% from nominal charge was used as the amount of fault induced for the test condition. This was chosen to give a significant fault level while maintaining the discharge pressure above the critical pressure of carbon dioxide 7.37 MPa. For the overcharged configuration a deviation of +10% from nominal charge was used. This was limited by safety concerns as a combination of high charge and fouling in the gas cooler can cause pressures high enough in the gas cooler to trigger the high pressure cutoff switch, which would then

disable the compressor. Table 8 shows the results of the test for the charge indicator. The results have been ordered from the lowest value to the highest.

Table 8. Fault indicator for deviation in charge level

Charge Level	Secondary Fault	Charge (no units)
Undercharge	Gas Cooler Fouling	-36.1
Undercharge	None	-36.1
Undercharge	Evaporator Fouling	-33.9
Undercharge	Compressor Valve	-19.9
Normal	Evaporator & Gas Cooler Fouling	-5.5
Normal	Evaporator Fouling	-4.8
Normal	Evaporator Fouling (Physical Blockage)	-3.4
Normal	None	-2.7
Normal	Compressor Valve & Evaporator Fouling	-2.1
Normal	Gas Cooler Fouling	-1.0
Normal	Gas Cooler Fouling	-0.4
Normal	Compressor Valve & Gas Cooler Fouling	2.2
Normal	Compressor Valve	2.3
Overcharge	Evaporator Fouling	5.6
Overcharge	None	12.4
Overcharge	Gas Cooler Fouling	13.4
Overcharge	Compressor Valve	18.0

For charge detection is no case of overlap, in which a normally charged condition has a higher fault indicator than that of a faulty charge. The evaporator fouling can falsely produce the effect of lowered charge or mask the appearance of overcharge; however, in order to cause a false positive or negative the magnitude of the fouling would have to be significantly greater than the 30% tested. Figure 30 shows the effect of

evaporator fouling on the charge sensor. No other secondary fault had significant impact on the virtual charge sensor.

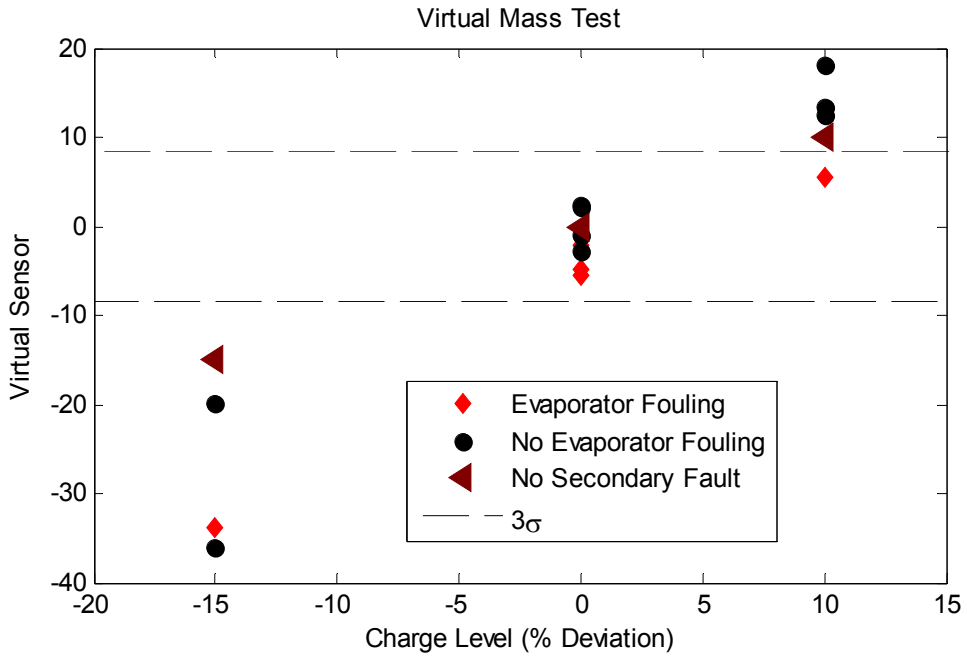

Figure 30. Effect of evaporator fouling on charge sensor

Gas Cooler Fouling

In simulating gas cooler fouling the gas cooler fan input control voltage was reduced by 30% which corresponds roughly to a 30% drop in mass flow rate. Also in a separate test, 40% of the gas cooler surface area was physically blocked to compare methods of simulating the fault. Unfortunately, there is no way of ensuring that the magnitude of the fault caused by the physical blockage corresponds to that of the reduction in fan speed. Larger amounts of fouling were not tested for safety reasons; the Danfoss 1410N compressor requires air cooling while in operation which is supplied by the gas cooler fan in the experimental system. As with all other faults, gas cooler

fouling was tested individually and with secondary faults present. Table 9 shows the results of the gas cooler air flow indicator given in order from smallest to largest.

Table 9. Gas cooler fouling indicator

Gas Cooler Fouling	Secondary Fault	Gas Cooler Air Flow (kg/min)
Yes	Overcharge	4.6
Yes	Undercharge	4.6
Yes	None	5.0
Yes (Physical Blockage)	None	5.3
Yes	Evaporator Fouling	5.4
Yes	Compressor Valve	5.9
No	Overcharge & Evaporator Fouling	6.2
No	Undercharge	6.4
No	Overcharge	6.8
No	Undercharge & Evaporator Fouling	7.0
No	Undercharge & Compressor Valve	7.1
No	None	7.5
No	Evaporator Fouling (Physical Blockage)	7.9
No	Compressor Valve	8.2
No	Overcharge & Compressor Valve	8.6
No	Evaporator Fouling	8.8
No	Compressor Valve & Evaporator Fouling	11.6

No overlap is present between the faulty and fault-free conditions. As mentioned in the theory section, this fault indicator is not completely independent of the compressor valve leakage fault. The compressor valve leakage fault renders the compressor map inaccurate and thus prevents its use. For that reason the data points where no compressor valve leakage was present are presented separately in Figure 31. A value of

zero on the x-axis indicates no fouling while a value of one indicates fouling is present. An uncertainty analysis was performed at the fault free point with the result of 13% uncertainty. The sources of error correspond to the uncertainties in the sensors as given by the manufacturers. Several assumptions were made in this analysis. The compressor map is assumed to be completely accurate, the refrigerant properties are assumed to perfectly match those of a pure substance with no adjustments for entrained oil, and there is assumed to be no bias due to the placement of sensors.

The majority of the points are within the range of the uncertainty. Those points outside of the uncertainty are there most likely due to violations of the aforementioned assumptions. Because the compressor map is no longer accurate when the compressor valve leakage is present, it is replaced by a revised version of the compressor valve leakage sensor.

Figure 32 shows the gas cooler fouling sensor without corrections for compressor valve leakage. The mass flow rate of air is significantly overestimated. Figure 33 shows the fouling sensor when the compressor valve leakage fault is included but corrected for. There is one outlier where the gas cooler air flow rate is overestimated, but otherwise the results are acceptable. The calculated uncertainty for points with the compressor valve leakage fault also increases. The uncertainty rises to 16% and this is with the assumption that the compressor valve leakage sensor is perfectly accurate, which it is not.

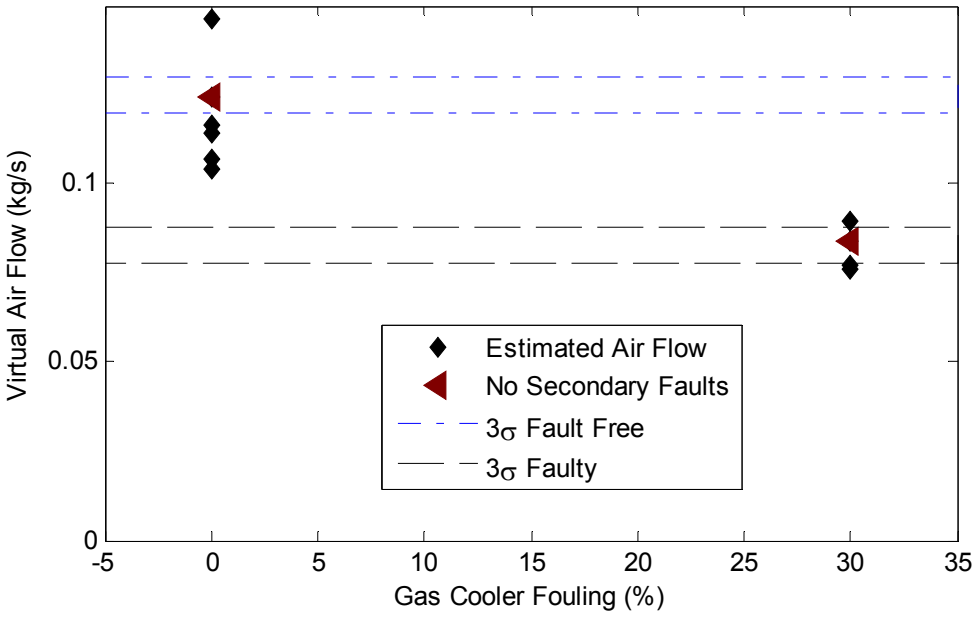

Figure 31. Gas cooler air fouling with compressor valve leakage excluded

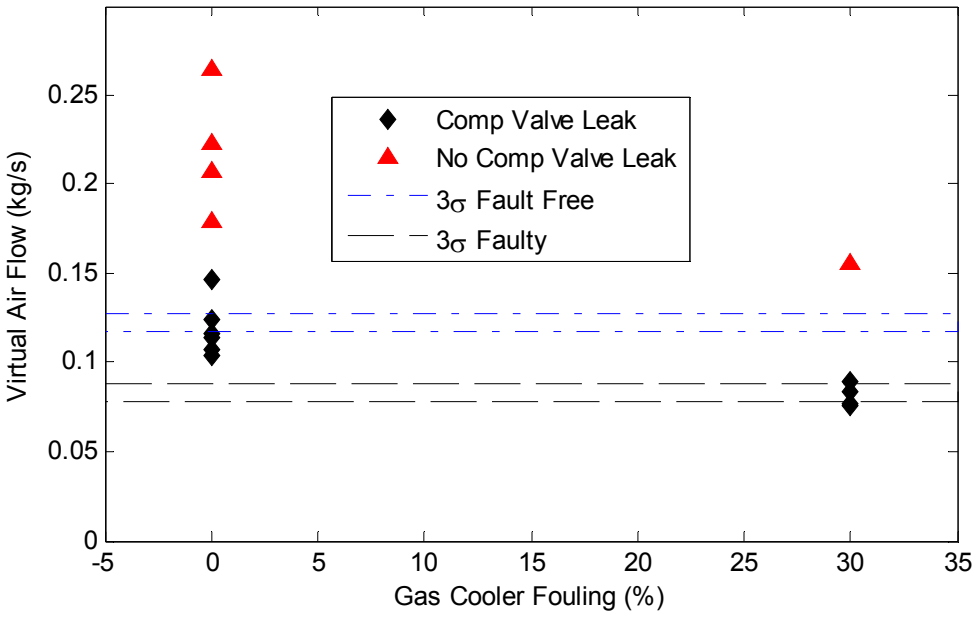

Figure 32. Gas cooler virtual sensor without corrections for compressor valve leakage

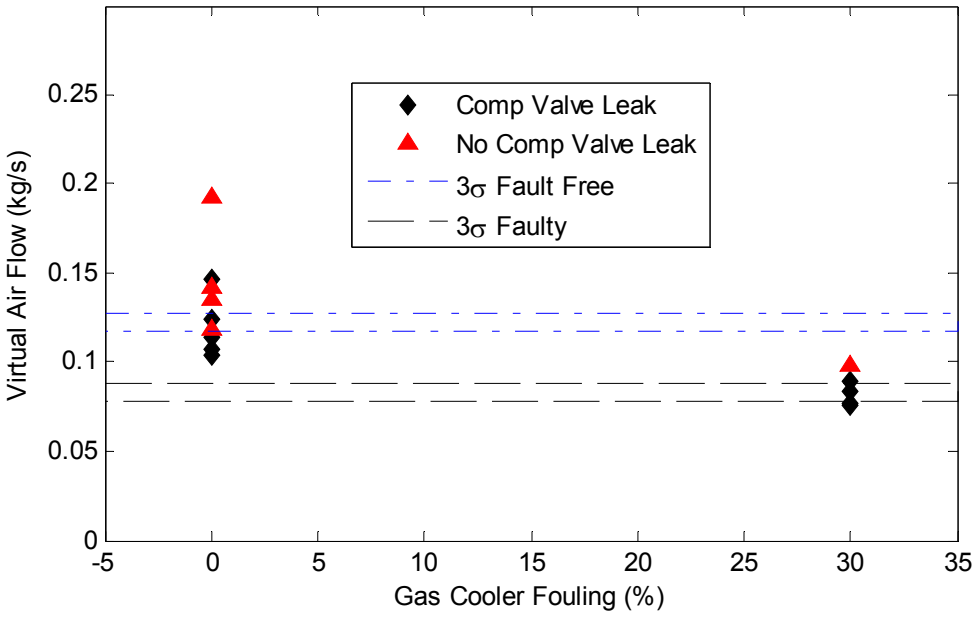

Figure 33. Gas cooler fouling with corrections for compressor valve leakage

Evaporator Fouling

For simulating evaporator fouling the evaporator fan input control voltage was decreased by 40% which is equivalent to a drop of one third in the mass flow rate of air. A physical blockage of 40% of the fan intake was separately tested for comparison. This level of fouling was chosen to give a significant fault level while maintaining an appropriate level of superheat. Larger amounts of fouling would have required adjusting the valve to keep superheat, thereby introducing a confounding factor. Table 10 shows the results of the virtual sensor for evaporator air flow.

Table 10. Evaporator fouling indicator

Evaporator Fouling	Secondary Fault	Evaporator Air Flow (kg/min)
Yes	None	2.1
Yes	Overcharge	2.2
Yes	Gas Cooler Fouling	2.6
Yes	Undercharge	3.2
Yes	Compressor Valve	3.4
Yes (Physical Blockage)	None	3.7
No	Overcharge & Gas Cooler Fouling	3.7
No	Overcharge	3.9
No	Gas Cooler Fouling (Physical Blockage)	4.0
No	Gas Cooler Fouling	4.0
No	None	4.2
No	Overcharge & Compressor Valve	4.5
No	Compressor Valve	4.5
No	Compressor Valve & Gas Cooler Fouling	4.7
No	Undercharge & Gas Cooler Fouling	4.7
No	Undercharge	4.9
No	Undercharge & Compressor Valve	5.2

Once again there is no overlap between the sensor's measurements for faulty and fault free conditions for the fouling simulated by a reduction in fan speed. As with gas cooler fouling, the presence of the compressor valve leakage fault renders the compressor map useless for mass flow rate. Figure 34 shows the virtual sensor for evaporator air flow without the compressor valve leakage present. The uncertainty associated with these measurements is 8%. The assumptions for this are the same as those for the gas cooler air flow virtual sensor with one additional assumption: the change in humidity in the air is ignored. This is an assumption of convenience since

humidity sensors are sometimes unreliable and need frequent calibration. These concerns limit their use in any practical implementation of a FDD method.

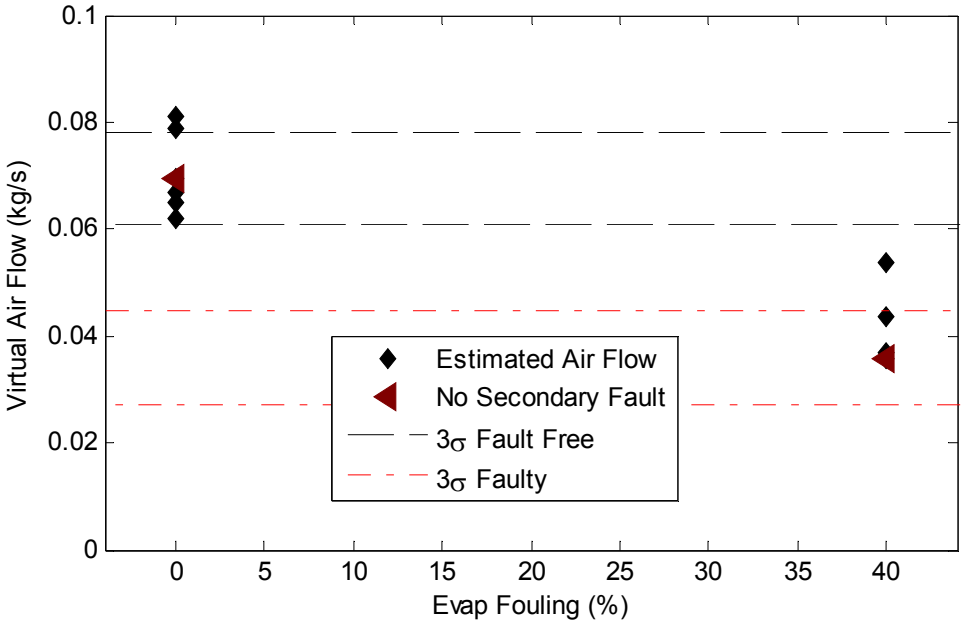

Figure 34. Evaporator fouling with compressor valve leakage excluded

Unlike the virtual sensor for gas cooler air flow, many of the data points are outside of the range of uncertainty. This is most likely due to the effects of moisture in the air condensing on the coils of the evaporator. As with the gas cooler air flow virtual sensor, the compressor valve leakage fault renders the compressor map inaccurate necessitating correction. Figure 35 shows the virtual sensor when no correction is made for the compressor valve leakage fault. The performance is extremely poor. Figure 36 shows the corrected data. Performance improves significantly. In the presence of the

compressor valve leakage uncertainty in the measurement of the evaporator air flow rate rises from 8% to 13%.

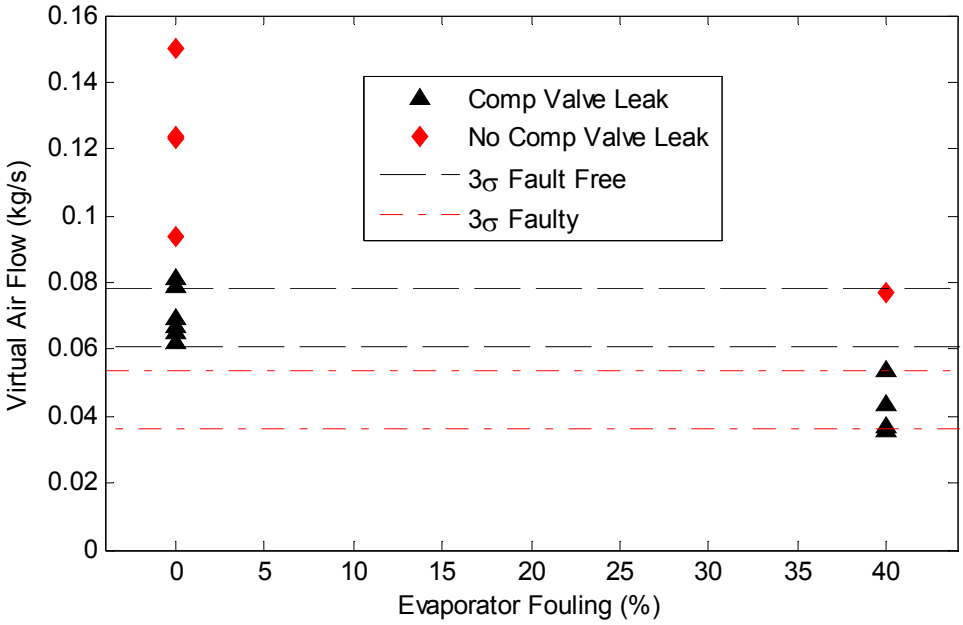

Figure 35. Evaporator fouling without corrections for compressor valve leakage

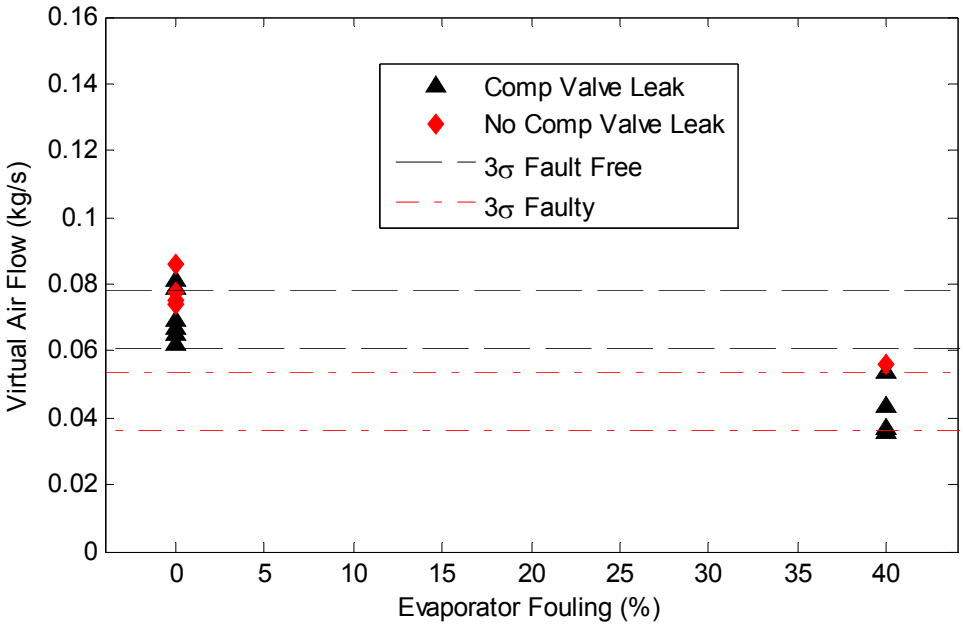

Figure 36. Evaporator fouling with corrections for compressor valve leakage

Compressor Valve Leakage

To simulate the compressor valve leakage fault a bypass valve was installed near the compressor. It is a needle valve which allows the flow of refrigerant from the exit of the compressor back to its entrance. During the simulations the valve was opened approximately one eighth of a turn. Because no mass flow meter is installed in the system, there is no way of measuring the relative magnitude of the fault outside of the virtual sensor. Table 11 gives the results of the virtual sensor.

Table 11. Compressor valve leakage indicator

Compressor Valve	Secondary Fault	ΔT_{ko} (°C)
Yes	Undercharge	4.7
Yes	Overcharge	3.3
Yes	None	2.3
Yes	Gas Cooler Fouling	2.2
No	None	1.2
Yes	Evaporator Fouling	1.2
No	Undercharge & Gas Cooler Fouling	1.1
No	Evaporator Fouling (Physical Blockage)	1.0
No	Gas Cooler Fouling (Physical Blockage)	0.9
No	Gas Cooler Fouling	0.8
No	Undercharge	0.4
No	Evaporator Fouling	0.4
No	Evaporator & Gas Cooler Fouling	-0.1
No	Undercharge & Evaporator Fouling	-0.1
No	Overcharge	-0.5
No	Overcharge & Gas Cooler Fouling	-0.7
No	Overcharge & Evaporator Fouling	-0.9

Of all the virtual sensors the performance of the compressor discharge temperature exhibited the poorest performance. There is some overlap present between faulty and fault-free conditions. The two largest sources of error are the compressor flow map and heat lost to the outside environment during compression. The flow map supplied by Danfoss was not very detailed. For each data point the discharge pressure was kept constant while the evaporation pressure was varied. As a result the pressure ratio was used as the only input variable as opposed to the suction and discharge pressures. Additionally, the compressor requires air cooling which increases the heat

loss to the surrounding environment which complicates the process of determining how much energy has been added to the refrigerant.

One observation in particular supports the notion that errors in the compressor map are the cause of this sensor's inaccuracy. Figure 37 shows that there is a strong clustering among the data points based off of the charge level. This is indicative of errors in the map because the pressure ratio undergoes the most change when refrigerant is added or removed from the system. Figure 38 illustrates the relationship that appears between the compressor outlet temperature residual and the pressure ratio. No uncertainty bars are included for the faulty-condition in Figure 37 as there is no a priori method of determining the magnitude of the fault outside of the virtual sensor.

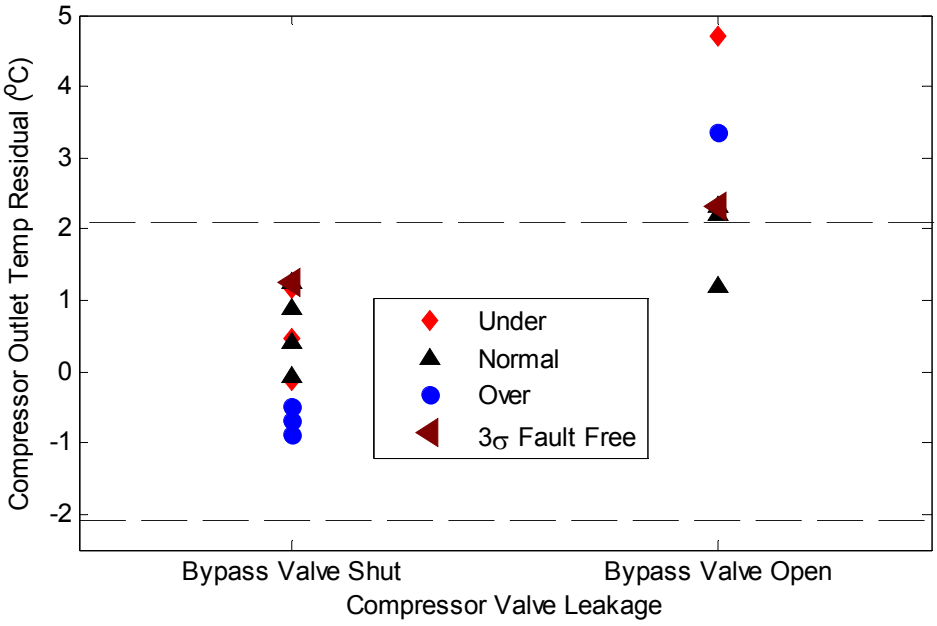

Figure 37. Compressor valve leakage and its dependence on charge

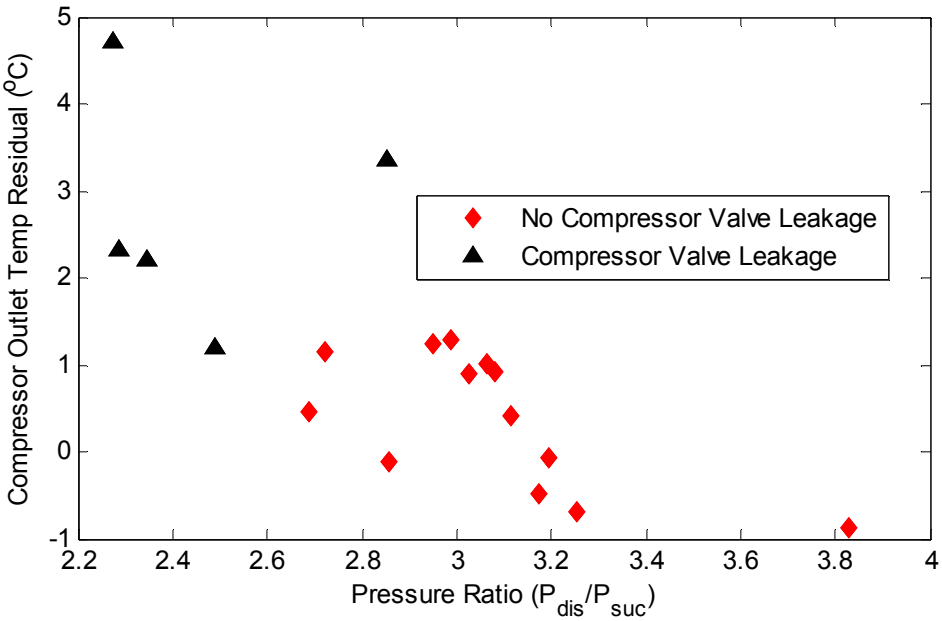

Figure 38. A comparison of compressor outlet temperature residual and pressure ratio

Transient Response of Virtual Sensors

Two of the faults, gas cooler and evaporator fouling, were chosen for dynamic testing of their virtual sensors. These two faults are the only ones which are likely to manifest quickly while the system is in operation. This was done to establish the speed at which sudden faults could be detected. Figure 39 and Figure 40 show the transient response of each sensor to a reduction in air speed indicative of fouling over the gas cooler and evaporator respectively. In both cases the dynamic response is good. The virtual sensor picks up the fault smoothly as the system dynamics settle with no aberrant behavior.

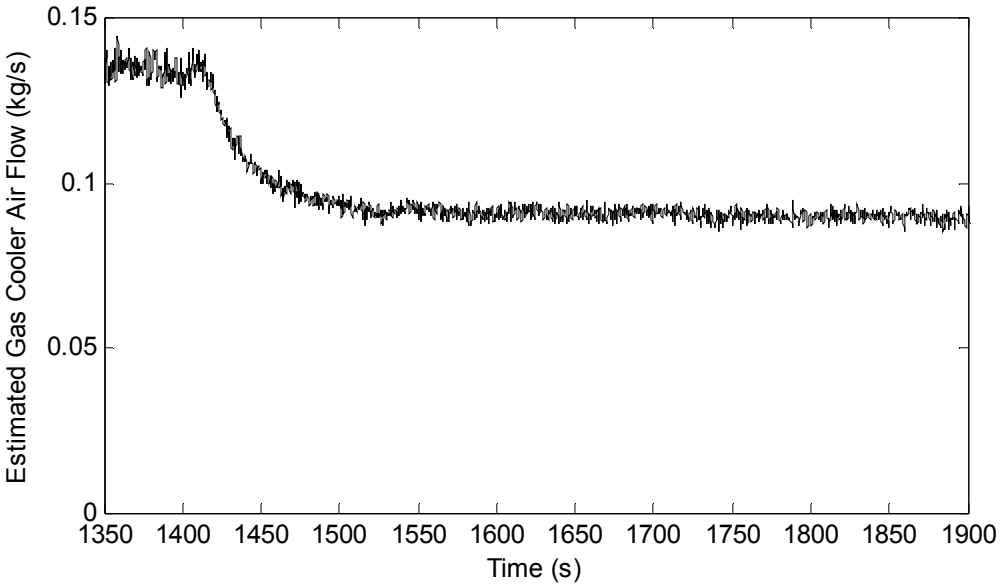

Figure 39. Transient response of gas cooler virtual sensor to sudden gas cooler fouling

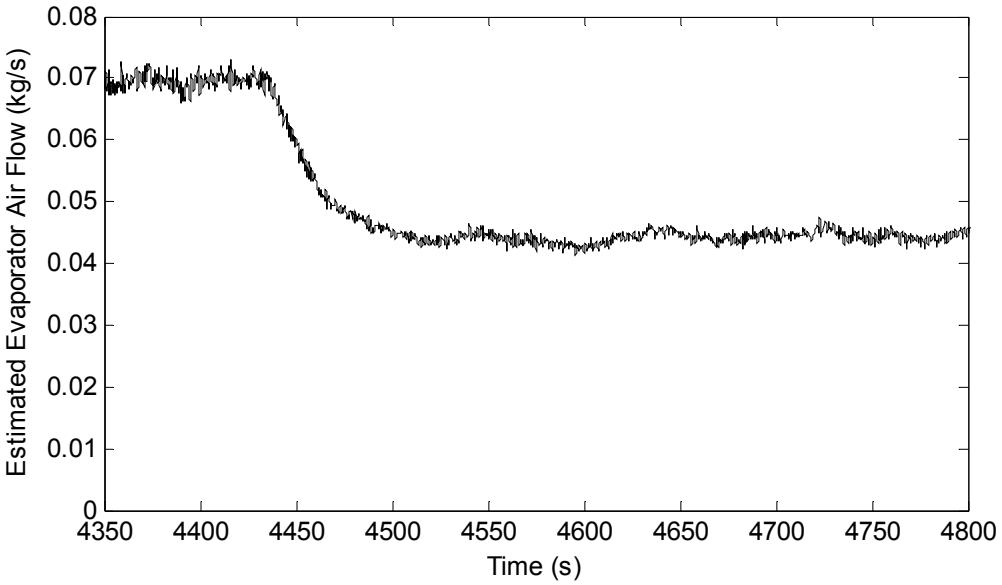

Figure 40. Transient response of evaporator virtual sensor to sudden evaporator fouling

While the system was operating at a fault-free condition, a step change was given to the valve to determine how each sensor would respond to excitation from the EEV. Figure 41, Figure 42, Figure 43, and Figure 44 show the reactions of each fault sensor to this step change. The step occurs at 50s. In each case there is no change in the fault sensor due to the valve step.

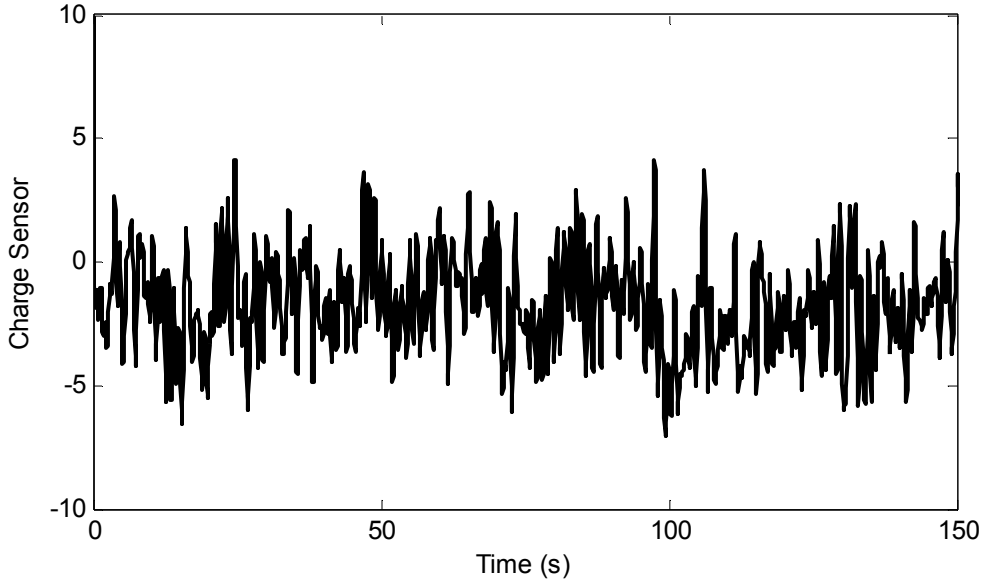

Figure 41. Response of the charge sensor to a valve step at fifty seconds

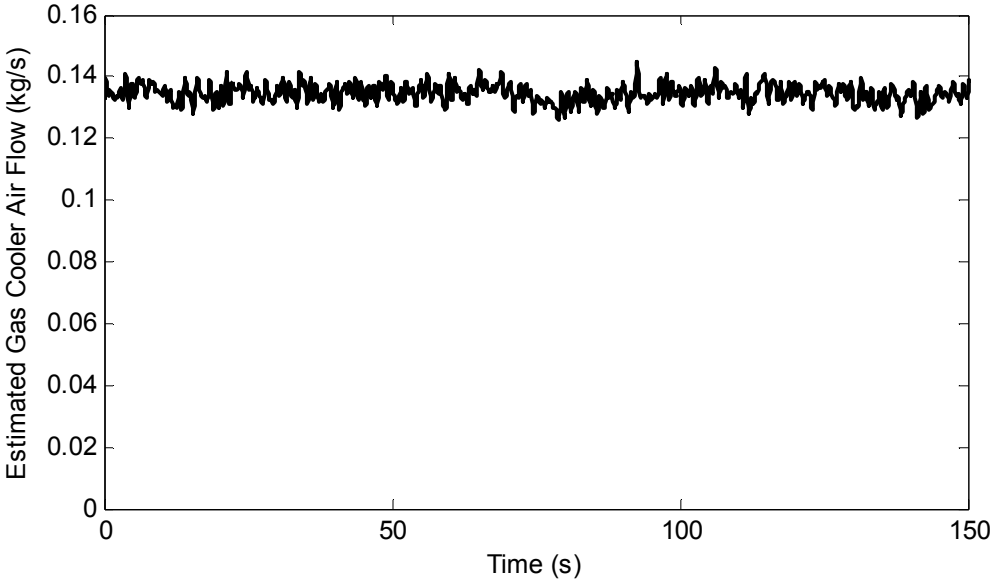

Figure 42. Response of the gas cooler virtual sensor to a valve step at fifty seconds

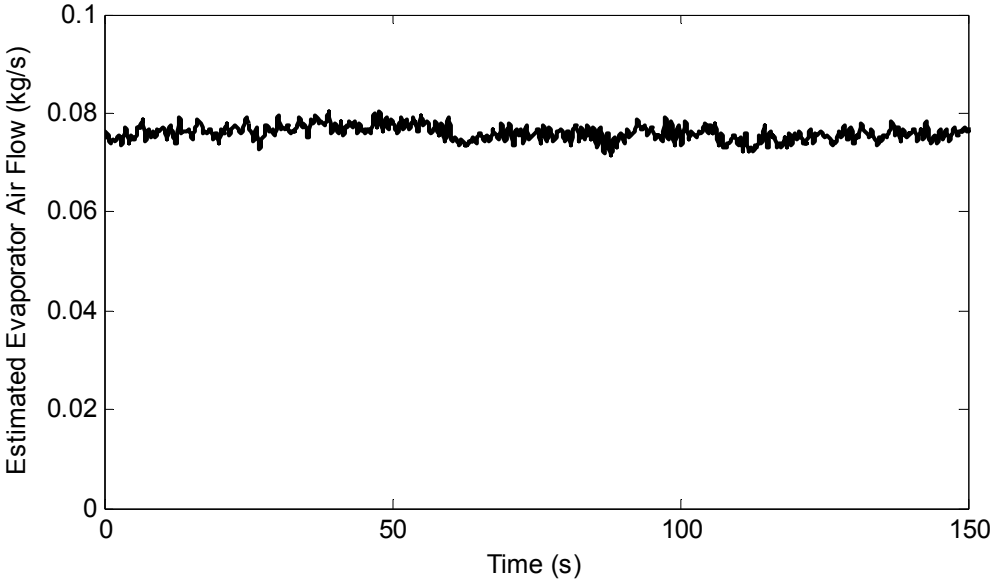

Figure 43. Response of the evaporator virtual sensor to a valve step at fifty seconds

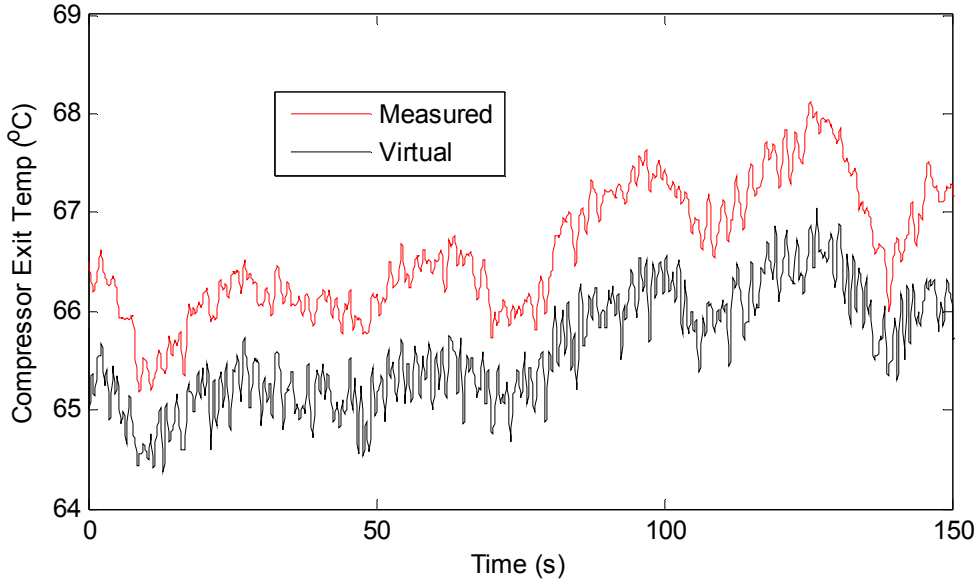

Figure 44. Response of the compressor outlet temperature sensor to a valve step at fifty seconds

Subcritical Comparison

As a benchmark for comparison, a similar set of tests using virtual sensors for static fault detection was run on a subcritical air conditioner. The major difference in these tests and those for the transcritical system is that no faults related to charge level were tested. This is simply because the subcritical system in question contains a receiver after the condenser. The receiver holds excess liquid refrigerant which negates the effect of any deviation in charge within certain limits. Only when the refrigerant inside the receiver is totally vapor or totally liquid would the effects of a change in charge be noticeable. Table 12 gives the order of testing. As earlier the designation of each fault as “Fault 1” or “Fault 2” is arbitrary.

Table 12. Order for subcritical tests

Order	Fault 1	Fault 2
1	None	None
2	Evaporator Fouling	None
3	Evaporator Fouling	Condenser Fouling
4	Condenser Fouling	None
5	Compressor Valve	Condenser Fouling
6	Compressor Valve	None
7	Compressor Valve	Evaporator Fouling

In each setting the air conditioner was allowed to come to steady state before a measurement was taken. Training data for the compressor valve leakage sensor was collected before these tests were run. Table 13 gives the results of each fault indicator at each testing point.

Table 13. Virtual sensor results for subcritical tests

Faults		Indicator		
Fault 1	Fault 2	Condenser Air Flow (kg/s)	Evaporator Air Flow (kg/s)	ΔT_{ko} (°C)
None	None	2.40	0.59	-0.4
Evaporator Fouling	None	2.66	0.46	-0.4
Evaporator Fouling	Condenser Fouling	1.67	0.48	0.1
Condenser Fouling	None	1.59	0.58	0.2
Compressor Valve	Condenser Fouling	1.55	0.55	3.8
Compressor Valve	None	2.32	0.55	3.3
Compressor Valve	Evaporator Fouling	2.40	0.44	3.8

As with the transcritical system, a test was performed to find the variation of the fault indicators in the operating region of the system. Combinations of high and low fan speeds for the condenser and evaporator fans were tested. The standard deviation of the steady state readings is shown in Table 14. The values three standard deviations from the fault-free point and the point with no secondary fault will be shown on the figures.

Table 14. Standard deviations of subcritical fault indicators in operating region

Indicator	σ (68%)	3σ (99.7%)
Condenser Fouling	0.13	0.38
Evaporator Fouling	0.01	0.03
Compressor Valve	0.34	1.02

Virtual Pressure Measurements

In a subcritical system both the suction and discharge pressures can be determined through temperature measurements in regions where the refrigerant is two-phase. In this system no thermocouple is positioned in the two-phase region of the condenser making the direct measurement of pressure necessary; however, the refrigerant at the inlet of the evaporator is always two-phase which allows for indirect calculation of the evaporator pressure. Figure 45 shows the correlation between the measured pressure and the virtual calculations based off of the saturation temperature. The agreement between the two is excellent.

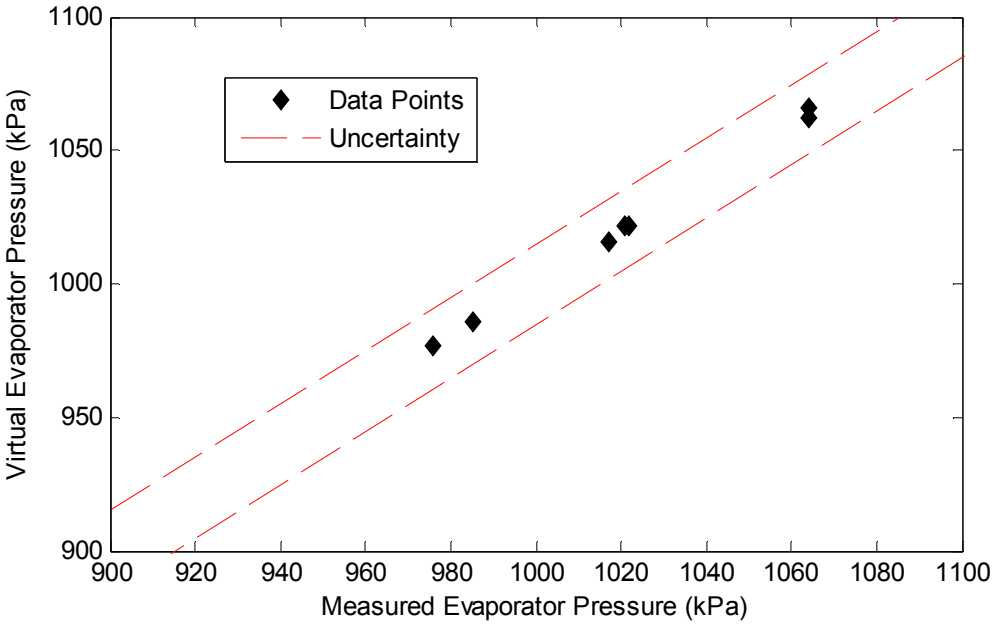

Figure 45. Virtual sensor for evaporator pressure

Condenser Fouling

For the simulation of condenser fouling the input control voltage to the condenser fan was dropped from 4V to 1V. This roughly corresponds to a 35% decrease in mass flow of air over the condenser. Table 15 gives the estimated condenser air flow in order of smallest to largest.

No overlap is present between faulty and fault free conditions and overall the grouping of the data points is excellent. Uncertainty analysis gives an error band of up to 22% based off of measurement errors. This large uncertainty is due to a small temperature drop in the air across the condenser which magnifies the already large uncertainty of the thermocouples. Because the pressure measurements are more accurate in the subcritical system, the change in uncertainty when the compressor valve leakage

fault is present is insignificant. Figure 46 shows a graphical representation of the condenser air flow sensor.

Table 15. Condenser fouling indicator

Condenser Fouling	Secondary Fault	Condenser Air Flow (kg/s)
Yes	Compressor Valve	1.55
Yes	None	1.59
Yes	Evaporator Fouling	1.67
No	Compressor Valve	2.32
No	None	2.40
No	Compressor Valve & Evaporator Fouling	2.40
No	Evaporator Fouling	2.66

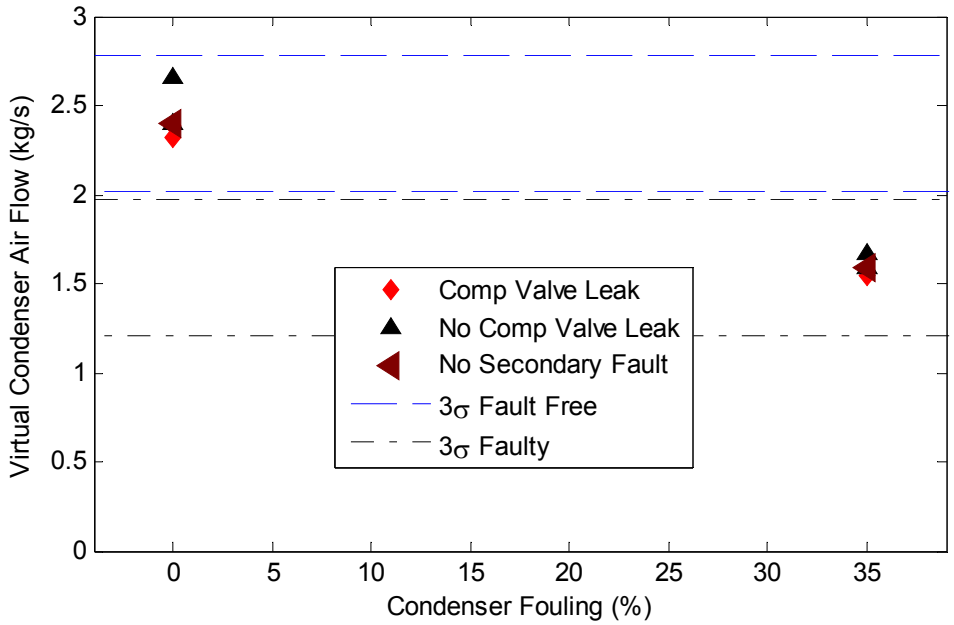

Figure 46. Subcritical condenser fouling virtual sensor

Evaporator Fouling

To simulate evaporator fouling the input control voltage to the evaporator fan was dropped from 5V to -5V. This roughly corresponds to a 30% decrease in the mass flow rate of air over the evaporator. Table 16 gives the results of the virtual sensor for evaporator air flow at each test level ordered from lowest to highest.

Table 16. Evaporator fouling indicator

Evaporator Fouling	Secondary Fault	Evaporator Air Flow (kg/s)
Yes	Compressor Valve	0.44
Yes	None	0.46
Yes	Condenser Fouling	0.48
No	Compressor Valve & Condenser Fouling	0.55
No	Compressor Valve	0.55
No	Condenser Fouling	0.58
No	None	0.59

There is no case of overlap between the faulty and fault-free conditions. As with the condenser fouling the grouping of the data is very good. The calculated uncertainty is 6%. It is much lower than that of the condenser because of the larger shift in air temperature across the evaporator. The addition of the compressor valve leak only increases the uncertainty of the measurement to 7%. Figure 47 gives a graphical representation of the virtual sensor for evaporator air flow.

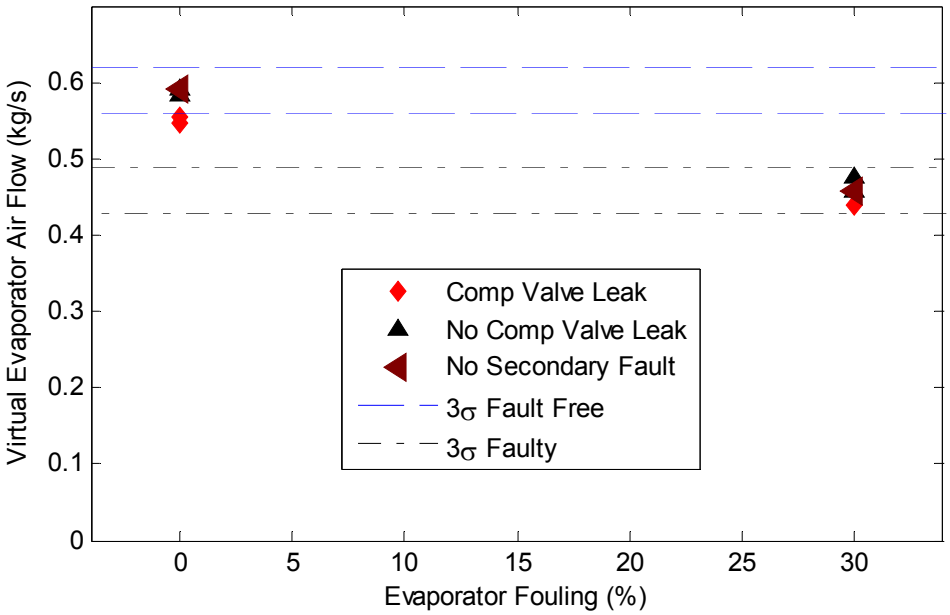

Figure 47. Subcritical evaporator fouling virtual sensor

Compressor Valve Leakage

In order to simulate compressor valve leakage on the subcritical air conditioner, a bypass valve was opened allowing flow from the discharge side of the compressor back to the suction side. The valve was opened a quarter of a turn to allow sufficient back flow. Table 17 shows the fault indicator for compressor valve leakage ordered from greatest temperature differential to smallest.

The results for this virtual sensor are excellent. There is close clustering in both the faulty and fault-free data points and a large gap between the two conditions. Uncertainty gives an error of ±0.8°C based off of measurement error. Figure 48 provides a graphical representation of the virtual sensor for compressor valve leakage.

Table 17. Compressor valve leakage indicator

Compressor Valve	Secondary Fault	ΔT_{ko} (°C)
Yes	Evaporator Fouling	3.8
Yes	Condenser Fouling	3.8
Yes	None	3.3
No	None	0.2
No	Evaporator & Condenser Fouling	0.1
No	Evaporator Fouling	-0.4
No	None	-0.4

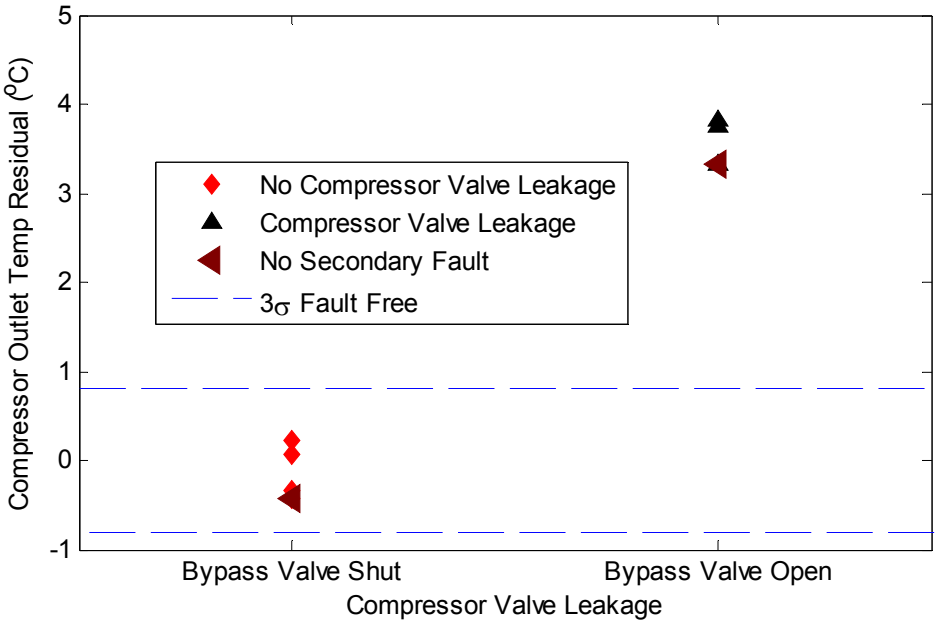

Figure 48. Subcritical compressor valve leakage virtual sensor

CONCLUSIONS

This thesis explored the feasibility of dynamic fault detection and diagnosis algorithms for transcritical vapor compression cycles. Step tests were performed under normal and faulty operating conditions for the most promising cases as identified by computer models. Responses were found to be largely first order. This implies that transient behavior adds little information to distinguish between faulty and fault-free behavior. The same tests were performed on a subcritical air conditioner and agree with the results for the transcritical refrigeration system.

A promising fault detection method for subcritical vapor compression cycles based off of the concept of virtual sensors was modified for use on a transcritical system. This technique reduces several common faults to the component level and allows for their detection to be independent of the incidence of other faults. The modifications preserve the general structure of the method while accounting for fundamental differences in the cycles. Testing of the virtual sensors for the transcritical system show that it provides acceptable ability to identify faults even when multiple faults are present. The same tests were performed on a subcritical air conditioner. The results agree with those of the transcritical cycle as well as previously published results for the virtual sensor method.

Future research may continue to focus on the practicality of this algorithm. Transferring the virtual sensor technique to a transcritical system introduced the need for a costly pressure sensor. While this hurts the economic feasibility of the method, many transcritical systems do have pressure sensors on the high side for control purposes.

REFERENCES

[1] Department of Energy, (2011, February 18). *End-Use Consumption of Electricity 2001*. Available: http://www.eia.doe.gov/emeu/recs/recs2001/enduse2001/enduse2001.html

[2] S. Katipamula and M. Brambley, "Methods for Fault Detection, Diagnostics, and Prognostics for Building Systems--A Review, Part I," *HVAC&R Research,* vol. 11, no. 1, pp. 3-25, 2005.

[3] S. Solomon, D. Qin, M. Manning, Z. Chen, M. Marquis, K.B. Averyt, M. Tignor and H.L. Miller, "Contribution of Working Group I to the Fourth Assessment Report of the Intergovernmental Panel on Climate Change," Cambridge University Press, New York2007.

[4] EPA. (2011, February 25). *Global Warming Potentials of ODS Substitutes*. Available: http://www.epa.gov/ozone/geninfo/gwps.html

[5] M. Comstock, J. Braun, and E. Groll, "A Survey of Common Faults for Chillers," *ASHRAE Transactions,* vol. 108, no. 1, pp. 819-825, 2002.

[6] S. Katipamula and M. Brambley, "Methods for Fault Detection, Diagnostics, and Prognostics for Building Systems--A Review, Part II," *HVAC&R Research,* vol. 11, no. 2, pp. 169-187, Apr 2005.

[7] A. Wilsky, "A Survey of Design Methods for Failure Detection in Dynamic Systems," *Automatica,* vol. 12, pp. 601-611, 1976.

[8] R. N. Clark, "Instrument Fault Detection," *IEEE Transactions on Aerospace and Electronic Systems,* vol. 14, no. 3, pp. 456-465, 1977.

[9] R. Isermann, "Process Fault Detection Based on Modeling and Estimation Methods--A Survey," *Automatica,* vol. 20, no. 4, pp. 387-404, 1984.

[10] J. Gertler, "Analytical Redundancy Methods in Fault Detection and Isolation," in *Proc. IFAC Symposium on Online Fault Detection and Supervision in the Chemical Process Industries,* Baden-Baden, Germany, 1991, pp. 9-21.

[11] P. Frank, "Fault Diagnosis in Dynamic Systems Using Analytical and Knowledge-Based Redundancy--A Survey and Some New Results," *Automatica,* vol. 26, no. 3, pp. 459-474, 1990.

[12] J. Gertler, "Fault Detection and Isolation Using Parity Relations," *Control Engineering Practice,* vol. 5, no. 5, pp. 653-661, 1997.

[13] J. Wagner and R. Shoureshi, "Failure Detection Diagnostics for Thermofluid Systems," *Journal of Dynamic Systems, Measurement, and Control,* vol. 114, no. 4, pp. 699-706, 1992.

[14] J. Liang and R. Du, "Model-Based Fault Detection and Diagnosis of HVAC Systems Using Support Vector Machine Method," *International Journal of Refrigeration,* vol. 30, no. 6, pp. 1104-1114, 2007.

[15] W.-Y. Lee, C. Park, and G. Kelly, "Fault Detection in an Air-Handling Unit Using Residual and Recursive Parameter Identification Methods," *ASHRAE Transactions,* vol. 102, no. 1, pp. 1-12, 1996.

[16] Y. Zhou and A. Dexter, "Estimating the Size of Incipient Faults in HVAC Equipment," *HVAC&R Research,* vol. 15, no. 1, pp. 151-163, 2009.

[17] M. Keir and A. Alleyne, "Dynamic Model-Based Fault Detection and Diagnosis Residual Considerations for Vapor Compression Systems," in *Proc. of the 2006 American Control Conference*, Minneapolis, 2006, pp. 4412-4417.

[18] T. I. Salsbury and R. C. Diamond, "Fault Detection in HVAC Systems Using Model-Based Feedforward Control," *International Journal of Refrigeration,* vol. 30, no. 6, pp. 1104-1114, 2007.

[19] A. Talukdar and A. Patra, "Dynamic Model-Based Fault Tolerant Control of Variable Air Volume Air Conditioning System," *HVAC&R Research,* vol. 16, no. 2, pp. 233-254, 2010.

[20] A. K. Halm-Owoo and K. O. Suen, "Applications of Fault Detection and Diagnostic Techniques for Refrigeration and Air Conditioning: A Review of Basic Principles," *Journal of Process Mechanical Engineering,* vol. 216, no. 3, pp. 121-132, 2002.

[21] Q. Zhou, S. Wang, and F. Xiao, "A Novel Strategy for the Fault Detection and Diagnosis of Centrifugal Chiller Systems," *HVAC&R Research,* vol. 15, no. 1, pp. 57-75, 2009.

[22] P. Haves, T. Salsbury, and J. Wright, "Condition Monitoring in HVAC Subsystems Using First Principle Models," *ASHRAE Transactions,* vol. 102, no. 1, pp. 519-527, 1996.

[23] S. A. Tassou and I. N. Grace, "Fault Diagnosis and Refrigerant Leak Detection in Vapour Compression Refrigeration Systems," *International Journal of Refrigeration,* vol. 28, no. 5, pp. 680-688, 2005.

[24] S. Wang and J. Cui, "Sensor Fault-Detection, Diagnosis and Estimation for Centrifugal Chiller Systems Using Principal Component Analysis Method," *Applied Energy,* vol. 82, no. 3, pp. 197-213, 2005.

[25] Y. Chen and L. Lan, "A Fault Detection Technique for Air-source Heat Pump Water Chiller/Heaters," *Energy and Buildings,* vol. 41, pp. 881-887, 2009.

[26] S. Li, "A Model-Based Fault Detection and Diagnostic Methodology for Secondary HVAC Systems," Ph.D dissertation, Mechanical Engineering, Drexel University, Philadelphia, 2009.

[27] H. Li and J. Braun, "An Improved Method for Fault Detection and Diagnosis Applied to Packaged Air Conditioners," *ASHRAE Transactions,* vol. 109, no. 2, pp. 683-692, 2003.

[28] H. Li and J. Braun, "A Methodology for Diagnosis Multiple Simultaneous Faults in Vapor-Compression Air Conditioners," *HVAC&R Research,* vol. 13, no. 2, pp. 369-395, 2007.

[29] D. Taylor and D. Corne, "An Investigation of the Negative Selection Algorithm for Fault Detection in Refrigeration Systems," *Lecture Notes in Computer Science: Artificial Immune Systems,* vol. 2787, pp. 34-45, 2003.

[30] H. Li and J. Braun, "Decoupling Features and Virtual Sensors for Diagnosis of Faults in Vapor Compression Air Conditioners," *International Journal of Refrigeration,* vol. 30, no. 3, pp. 546-564, 2007.

[31] H. Li and J. Braun, "Development, Evaluation, and Demonstration of a Virtual Refrigerant Charge Sensor," *HVAC&R Research,* vol. 15, no. 1, pp. 117-136, 2009.

[32] A. Wichman and J. Braun, "Fault Detection and Diagnostics for Commercial Coolers and Freezers," *HVAC&R Research,* vol. 15, no. 1, pp. 77-99, 2009.

[33] H. Li and J. Braun, "Virtual Refrigerant Pressure Sensors for Use in Monitoring and Fault Diagnosis of Vapor-Compression Equipment," *HVAC&R Research,* vol. 15, no. 3, pp. 597-616, 2009.

[34] J. R. Thome and J. E. Hajal, "Flow Boiling Heat Transfer to Carbon Dioxide: General Prediction Method," *International Journal of Refrigeration,* vol. 27, no. 3, pp. 294-301, 2004.

[35] N. Kattan, J. R. Thome, and D. Favrat, "Flow Boiling in Horizontal Tubes. Part 3: Development of a New Heat Transfer Model Based on Flow Patterns," *Journal of Heat Transfer,* vol. 120, no. 1, pp. 156-165, 1998.

[36] V. Gnielinski, "New Equations for Heat and Mass Transfer in Turbulent Pipe and Channel Flow," *International Chemical Engineering,* vol. 16, pp. 359-368, 1976.

[37] S. H. Yoon, J. H. Kim, Y. W. Hwang, M. S. Kim, K. Min, and Y. Kim, "Heat Transfer and Pressure Drop Characteristics During the In-Tube Cooling Process of Carbon Dioxide in the Supercritical Region," *International Journal of Refrigeration,* vol. 26, no. 8, pp. 857-864, 2003.

[38] N. Hariharan, "Parameter Estimation of Dynamic Air-Conditioning Component Models Using Limited Sensor Data," M.S. thesis, Mechanical Engineering, Texas A&M University, College Station, 2010.

[39] B. Rasmussen and A. Alleyne, "Control Oriented Modeling of Transcritical Vapor Compression Systems," *Transactions of the ASME,* vol. 126, no. 1, pp. 54-64, March 2004.

[40] P. G. Mehta and B. A. Eisenhower, "Computational Modeling and Analysis of Multiple Steady States in Vapor Compression Systems," *Transactions of the ASME,* vol. 2, pp. 132-140, 2007.

[41] A. Gupta, "Reduced Order Modeling of Heat Exchangers Using High Order Finite Control Volume Models," Record of Study, Mechanical Engineering, Texas A&M University, College Station, 2007.

APPENDIX

The complete derivation of the governing equations for the FCV heat exchanger follows. Details of this derivation have been taken from the work of Gupta [41]. The derivation of these models starts with the conservation of energy and mass equations. Eq. 16 gives the energy balance for a particular node in its most general form, while Eq. 17 shows the conservation expanded and applied to each control volume.

$$\dot{U}_k = \dot{H}_{k-1} - \dot{H}_k + \dot{Q}_{w,k} \tag{16}$$

$$\begin{bmatrix} \dot{U}_1 \\ \vdots \\ \dot{U}_k \\ \vdots \\ \dot{U}_n \end{bmatrix} = \begin{bmatrix} \dot{m}_{in}h_{in} - \dot{m}_1 h_1 + \alpha_{i,1}A_i(T_{w,1} - T_{r,1}) \\ \vdots \\ \dot{m}_{k-1}h_{k-1} - \dot{m}_k h_k + \alpha_{i,k}A_i(T_{w,k} - T_{r,k}) \\ \vdots \\ \dot{m}_{n-1}h_{n-1} - \dot{m}_n h_n + \alpha_{i,n}A_i(T_{w,n} - T_{r,n}) \end{bmatrix} \tag{17}$$

Here U refers to internal energy, H is the enthalpy, Q_w is the heat from the pipe walls to the refrigerant, $\dot{m}$ is the mass flow rate of the refrigerant, α_i is the internal convective heat transfer coefficient, A_i is the internal pipe wall area for a control volume, T_w is the pipe wall temperature, and T_r is the refrigerant temperature.

The next set of equations is the energy balance applied to the pipe walls. Eq. 18 gives the general form of the pipe wall energy balance. Once it is applied to individual control volumes and substitutions are made, Eq. 19 results.

$$\dot{E}_w = \dot{Q}_a - \dot{Q}_w \tag{18}$$

$$\begin{bmatrix} \dot{E}_{w,1} \\ \vdots \\ \dot{E}_{w,k} \\ \vdots \\ \dot{E}_{w,n} \end{bmatrix} = \begin{bmatrix} \alpha_{o,1} A_o (T_{a,1} - T_{w,1}) - \alpha_{i,1} A_i (T_{w,1} - T_{r,1}) \\ \vdots \\ \alpha_{o,k} A_o (T_{a,k} - T_{w,k}) - \alpha_{i,k} A_i (T_{w,k} - T_{r,k}) \\ \vdots \\ \alpha_{o,n} A_o (T_{a,n} - T_{w,n}) - \alpha_{i,n} A_i (T_{w,n} - T_{r,n}) \end{bmatrix} \tag{19}$$

Here E_w is the energy in the pipe wall, Q_a is the heat from the air to the pipe walls, α_o is the external convective heat transfer coefficient, A_o is the external pipe wall area, and T_a is the inlet air temperature.

The final cog needed to start the derivation is the conservation of mass for each control volume. Eq. 20 shows the refrigerant mass balance. The variable $\dot{m}_{hx}$ corresponds to the rate of change of the refrigerant mass in a control volume within the heat exchanger. Eq. 21 gives the overall mass balance for the heat exchanger.

$$\begin{bmatrix} \dot{m}_{hx,1} \\ \vdots \\ \dot{m}_{hx,k} \\ \vdots \\ \dot{m}_{hx,n} \end{bmatrix} = \begin{bmatrix} \dot{m}_{in} - \dot{m}_1 \\ \vdots \\ \dot{m}_{k-1} - \dot{m}_k \\ \vdots \\ \dot{m}_{n-1} - \dot{m}_{out} \end{bmatrix} \tag{20}$$

$$\dot{m}_{hx} = \dot{m}_{in} - \dot{m}_{out} \tag{21}$$

These three balances can be combined to one large equation which will contain all the needed information. Eq. 22 gives the conservation laws combined to a single set of vectors.

$$\begin{bmatrix} \dot{U}_1 \\ \vdots \\ \dot{U}_k \\ \vdots \\ \dot{U}_n \\ \dot{m}_{hx} \\ \dot{E}_{w,1} \\ \vdots \\ \dot{E}_{w,k} \\ \vdots \\ \dot{E}_{w,n} \end{bmatrix} = \begin{bmatrix} \dot{m}_{in}h_{in} - \dot{m}_1 h_1 + \alpha_{i,1}A_i(T_{w,1} - T_{r,1}) \\ \vdots \\ \dot{m}_{k-1}h_{k-1} - \dot{m}_k h_k + \alpha_{i,k}A_i(T_{w,k} - T_{r,k}) \\ \vdots \\ \dot{m}_{n-1}h_{n-1} - \dot{m}_n h_n + \alpha_{i,n}A_i(T_{w,n} - T_{r,n}) \\ \dot{m}_{in} - \dot{m}_{out} \\ \alpha_{o,1}A_o(T_{a,1} - T_{w,1}) - \alpha_{i,1}A_i(T_{w,1} - T_{r,1}) \\ \vdots \\ \alpha_{o,k}A_o(T_{a,k} - T_{w,k}) - \alpha_{i,k}A_i(T_{w,k} - T_{r,k}) \\ \vdots \\ \alpha_{o,n}A_o(T_{a,n} - T_{w,n}) - \alpha_{i,n}A_i(T_{w,n} - T_{r,n}) \end{bmatrix} \tag{22}$$

To create the final form of the heat exchanger model Eqs. 17 and 19 are combined and Eq. 20 will be used to remove unnecessary terms. Additionally, a great deal of substitutions in terms of fluid properties and their derivatives must be made. The goal of these substitutions is to leave only enthalpy and pressure as fluid states. They will now be detailed.

To begin the overall properties of the refrigerant must be replaced by the specific properties for ease of calculation. Eq 23 and 24 give the internal energy of each control volume and its derivative in specific form. Eq. 25 and 26 substitute to replace mass and density terms.

$$U_k = m_{hx,k}u_k \tag{23}$$

$$\dot{U}_k = \dot{m}_{hx,k}u_k + m_{hx,k}\dot{u}_k \tag{24}$$

$$\dot{U}_k = V_{hx}(\dot{\rho}_k u_k + \rho_k \dot{u}_k) \tag{25}$$

$$\dot{U}_k = V_{hx}\left[\left(\left.\frac{\partial \rho_k}{\partial P_k}\right|_{h_k} \dot{P}_{hx} + \left.\frac{\partial \rho_k}{\partial h_k}\right|_{P_k} \dot{h}_k\right) u_k + \left(\left.\frac{\partial u_k}{\partial P_k}\right|_{h_k} \dot{P}_{hx} + \left.\frac{\partial u_k}{\partial h_k}\right|_{P_k} \dot{h}_k\right) \rho_k\right] \tag{26}$$

Here V_{hx} is the internal volume of a section of the heat exchanger, ρ is the density of a control volume, and P_{hx} is the pressure of the heat exchanger.

The internal energy of the refrigerant must be replaced by the enthalpy of the refrigerant. To do this the formal definition of enthalpy will be used as given by Eq. 27. When this is placed in Eq. 26 and simplified, Eq. 28 results. This completes the substitutions needed for the refrigerant energy balance.

$$h_k = u_k + \frac{P_{hx}}{\rho_k} \tag{27}$$

$$\dot{U}_k = V_{hx}\left[\left(\left.\frac{\partial \rho_k}{\partial P_k}\right|_{h_k} h_k - 1\right) \dot{P}_{hx} + \left(\left.\frac{\partial \rho_k}{\partial h_k}\right|_{P_k} h_k + \rho_k\right) \dot{h}_k\right] \tag{28}$$

Once the internal energy has been removed, the next step is to replace $\dot{m}_{hx}$ in Eq. 22 with another expression. Eq. 29 gives $\dot{m}_{hx}$ as a sum of the individual control volumes. Each of these intermediate terms can be defined by Eq. 30. When the proper substitutions are performed Eqs. 31 and 32 result which allows removal of $\dot{m}_{hx}$ from Eq. 22.

$$\dot{m}_{hx} = \sum_{i=1}^{n} \dot{m}_{hx,i} \tag{29}$$

$$\dot{m}_{hx,k} = V_{hx}\dot{\rho}_k \tag{30}$$

$$\dot{m}_{hx,k} = V_{hx}\left(\left.\frac{\partial \rho_k}{\partial P_{hx}}\right|_{h_k} \dot{P}_{hx} + \left.\frac{\partial \rho_k}{\partial h_k}\right|_{P_{hx}} \dot{h}_k \right) \tag{31}$$

$$\dot{m}_{hx} = V_{hx}\sum_{i=1}^{n}\left(\left.\frac{\partial \rho_i}{\partial P_{hx}}\right|_{h_i} \dot{P}_{hx} + \left.\frac{\partial \rho_i}{\partial h_i}\right|_{P_{hx}} \dot{h}_i \right) \tag{32}$$

Now the time derivative of wall energy must be made a function of the wall temperature. This is a simple change if a uniform wall temperature is assumed for a given node. Eq. 33 displays the needed substitution.

$$\dot{E}_{w,k} = C_{p,w}\rho_w V_w \dot{T}_w \tag{33}$$

Here $C_{p,w}$ is the wall's specific heat, ρ_w is the density of the wall, and V_w is the wall's volume for that node.

The final step in the derivation is to remove the intermediate mass flow terms from the right side of Eq. 17. This is accomplished using Eq. 20. Eq. 34 shows the substitution needed to replace $\dot{m}_k$. When this is placed into Eq. 28, Eq. 35 results. Moving all time derivatives to the left hand side results in Eq. 36.

$$\dot{m}_k = \dot{m}_{in} - V_{hx}\sum_{i=1}^{k}\left(\left.\frac{\partial \rho_i}{\partial P_{hx}}\right|_{h_i} \dot{P}_{hx} + \left.\frac{\partial \rho_i}{\partial h_i}\right|_{P_{hx}} \dot{h}_i \right) \tag{34}$$

$$\dot{U}_k = V_{hx}\left[\left(\left.\frac{\partial \rho_k}{\partial P_{hx}}\right|_{h_k} h_k - 1\right)\dot{P}_{hx} + \left(\left.\frac{\partial \rho_k}{\partial h_k}\right|_{P_{hx}} h_k + \rho_k\right)\dot{h}_k\right] =$$

$$\dot{m}_{in}(h_{k-1} - h_k) + V_{hx}h_{k-1}\sum_{i=1}^{k-1}\left(\left.\frac{\partial \rho_i}{\partial P_{hx}}\right|_{h_i}\dot{P}_{hx} + \left.\frac{\partial \rho_i}{\partial h_i}\right|_{P_{hx}}\dot{h}_i\right) - \tag{35}$$

$$V_{hx}h_k\sum_{i=1}^{k}\left(\left.\frac{\partial \rho_i}{\partial P_{hx}}\right|_{h_i}\dot{P}_{hx} + \left.\frac{\partial \rho_i}{\partial h_i}\right|_{P_{hx}}\dot{h}_i\right) + \alpha_{i,k}A_i(T_{w,k} - T_{r,k})$$

$$V_{hx}\left[-\left((h_k - h_{k-1})\sum_{i=1}^{k}\left(\left.\frac{\partial \rho_i}{\partial P_{hx}}\right|_{h_i}\right) + 1\right)\dot{P}_{hx} + \rho_k\dot{h}_k + (h_{k-1} - h_k)\sum_{i=1}^{k-1}\left(\left.\frac{\partial \rho_i}{\partial h_i}\right|_{P_{hx}}\dot{h}_i\right)\right] \tag{36}$$

$$= \dot{m}_{in}(h_{k-1} - h_k) + \alpha_{i,k}A_i(T_{w,k} - T_{r,k})$$

With that all necessary replacements have been made to put the equations into their final form.

$$Z(x,u)\dot{x} = f(x,u) \tag{37}$$

$$x = \begin{bmatrix} P & h_1 & \dots & h_k & \dots & h_n & T_{w,1} & \dots & T_{w,k} & \dots & T_{w,n} \end{bmatrix}^T \tag{38}$$

$$u = \begin{bmatrix} \dot{m}_{in} & \dot{m}_{out} & h_{in} & T_{air,in} & \dot{m}_{air} \end{bmatrix}^T \tag{39}$$

The *Z* matrix can be broken down into its constituent parts. Eq. 40 shows that *Z* is a block matrix. Definitions of all of the sub-matrices can be found in Eqs. 41 to 49. *f(x,u)* is a *2n+1* vector which is shown in Eq. 50.

$$Z(x,u)=\begin{bmatrix} Z_{11,(nX1)} & Z_{12,(nXn)} & 0 \\ Z_{21,(1X1)} & Z_{22,(1Xn)} & 0 \\ 0 & 0 & Z_{33,(nXn)} \end{bmatrix}_{(2n+1)X(2n+1)} \tag{40}$$

$$Z_{11}=\begin{bmatrix} Z_{11}^{1} \\ \vdots \\ Z_{11}^{k} \\ \vdots \\ Z_{11}^{n} \end{bmatrix}_{nX1} \tag{41}$$

$$Z_{11}^{1}=-V_{hx} \tag{42}$$

$$Z_{11}^{k}=-V_{hx}\left((h_k-h_{k-1})\sum_{i=1}^{k}\left(\left.\frac{\partial\rho_i}{\partial P_{hx}}\right|_{h_i}\right)+1\right) \tag{43}$$

$$Z_{12}=\begin{bmatrix} Z_{12}^{11} & 0 & \cdots & 0 & 0 \\ \vdots & \ddots & 0 & \cdots & \vdots \\ Z_{12}^{k1} & \cdots & Z_{12}^{kk} & 0 & 0 \\ \vdots & & & \ddots & \vdots \\ Z_{12}^{n1} & \cdots & \cdots & Z_{12}^{n(n-1)} & Z_{12}^{nn} \end{bmatrix}_{nXn} \tag{44}$$

$$Z_{12}^{kk}=V_{hx}\rho_k \tag{45}$$

$$Z_{12}^{ki}=V_{hx}(h_{k-1}-h_k)\left.\frac{\partial\rho_i}{\partial h_i}\right|_{P_{hx}} \tag{46}$$

$$Z_{21}=V_{hx}\sum_{i=1}^{n}\left(\left.\frac{\partial\rho_i}{\partial P_{hx}}\right|_{h_i}\right) \tag{47}$$

$$Z_{22} = \left[V_{hx} \left. \frac{\partial \rho_1}{\partial P_{hx}} \right|_{h_1} \quad \cdots \quad V_{hx} \left. \frac{\partial \rho_k}{\partial P_{hx}} \right|_{h_k} \quad \cdots \quad V_{hx} \left. \frac{\partial \rho_n}{\partial P_{hx}} \right|_{h_n} \right]_{1Xn} \tag{48}$$

$$Z_{33} = diag\left\{ (C_p \rho V)_{w,i} \right\}_{nXn} \tag{49}$$

$$f(x,u) = \begin{bmatrix} \dot{m}_{in}(h_{in} - h_1) + \alpha_{i,1} A_i (T_{w,1} - T_{r,1}) \\ \vdots \\ \dot{m}_{in}(h_{k-1} - h_k) + \alpha_{i,k} A_i (T_{w,k} - T_{r,k}) \\ \vdots \\ \dot{m}_{in}(h_{n-1} - h_n) + \alpha_{i,n} A_i (T_{w,n} - T_{r,n}) \\ \dot{m}_{in} - \dot{m}_{out} \\ \alpha_{o,1} A_o (T_{a,1} - T_{w,1}) - \alpha_{i,1} A_i (T_{w,1} - T_{r,1}) \\ \vdots \\ \alpha_{o,k} A_o (T_{a,k} - T_{w,k}) - \alpha_{i,k} A_i (T_{w,k} - T_{r,k}) \\ \vdots \\ \alpha_{o,n} A_o (T_{a,n} - T_{w,n}) - \alpha_{i,n} A_i (T_{w,n} - T_{r,n}) \end{bmatrix}_{(2n+1)X1} \tag{50}$$

Heat Transfer Correlations

Two sets of correlations are used in the evaporator. The correlation of Thome and Hajal is used to calculate the internal coefficient in the two-phase regions [34]. It is a version of the general evaporative heat transfer correlation derived by Kattan et al. adapted specifically for carbon dioxide [35]. For the region which contains pure vapor, a correlation by Gnielinski for general vapor flow in heat exchangers [36]. For the gas cooler only one heat transfer correlation was required, that of Yoon et al. for use in supercritical cooling of carbon dioxide [37]. The equations governing these heat transfer coefficients will now be presented.

The Gnielinski Correlation

The Gnielinski correlation can be broken into two pieces. The first and simpler of these is the correlation for turbulent flow typically with a Reynolds number above 2400. Eq. 51 shows the form for the correlation.

$$Nu = \frac{f}{8}\frac{(\mathrm{Re}-1000)\,\mathrm{Pr}}{\left[1+12.7\left(\frac{f}{8}\right)^{\frac{1}{2}}\left(\mathrm{Pr}^{\frac{2}{3}}-1\right)\right]} \tag{51}$$

Here f is the friction factor, Re is the Reynolds number, Nu is the Nusselt number, and Pr is the Prandtl number.

For turbulent flow several equations are used in conjunction. Eqs. 52 through 63 give all necessary information. Each equation can be solved using the values calculated from the previous equations.

$$Nu_l = 4.364 \tag{52}$$

$$\mathrm{Re}_h = 2400 \tag{53}$$

$$\mathrm{Re}_l = 1000 + Nu_l \frac{1+12.7\left(\frac{f}{8}\right)^{0.5}\left(\mathrm{Pr}^{2/3}-1\right)}{\mathrm{Pr}\left(\frac{f}{8}\right)} \tag{54}$$

$$Nu_a = \frac{f}{8}\frac{(2400-1000)\,\mathrm{Pr}}{\left[1+12.7\left(\frac{f}{8}\right)^{\frac{1}{2}}\left(\mathrm{Pr}^{\frac{2}{3}}-1\right)\right]} \tag{55}$$

$$Nu_b = \frac{f}{8}\frac{(2405-1000)\,\mathrm{Pr}}{\left[1+12.7\left(\frac{f}{8}\right)^{\frac{1}{2}}\left(\mathrm{Pr}^{\frac{2}{3}}-1\right)\right]} \tag{56}$$

$$Nu_a = \frac{f}{8}\frac{(2410-1000)\,\mathrm{Pr}}{\left[1+12.7\left(\frac{f}{8}\right)^{\frac{1}{2}}\left(\mathrm{Pr}^{\frac{2}{3}}-1\right)\right]} \tag{57}$$

$$\delta Nu = \frac{4Nu_b - Nu_c - 3Nu_a}{10} \tag{58}$$

$$a = -\frac{2Nu_h - 2Nu_l - \delta Nu(\mathrm{Re}_h - \mathrm{Re}_l)}{\left(\mathrm{Re}_h - \mathrm{Re}_l\right)^3} \tag{59}$$

$$b = \frac{3\,\mathrm{Re}_h(Nu_h - Nu_l) - \delta Nu\,\mathrm{Re}_h^2 + 3Nu_h\,\mathrm{Re}_l - \delta Nu\,\mathrm{Re}_h\,\mathrm{Re}_l^2 + 2\delta Nu\,\mathrm{Re}_l^2}{\left(\mathrm{Re}_h - \mathrm{Re}_l\right)^3} \tag{60}$$

$$c = -\frac{6\,\mathrm{Re}_h\,\mathrm{Re}_l(Nu_h - Nu_l) - 2\delta Nu\,\mathrm{Re}_h^2\,\mathrm{Re}_l + \delta Nu\,\mathrm{Re}_h\,\mathrm{Re}_l^2 + \delta Nu\,\mathrm{Re}_l^3}{\left(\mathrm{Re}_h - \mathrm{Re}_l\right)^3} \tag{61}$$

$$d = -\frac{\begin{array}{c}-Nu_l\,\mathrm{Re}_h + 3\,\mathrm{Re}_h\,\mathrm{Re}_l(Nu_l\,\mathrm{Re}_h - Nu_h\,\mathrm{Re}_l) \\ +\delta Nu(\mathrm{Re}_h^2\,\mathrm{Re}_l^2 - \mathrm{Re}_h\,\mathrm{Re}_l^3) + Nu_h\,\mathrm{Re}_l^3\end{array}}{\left(\mathrm{Re}_h - \mathrm{Re}_l\right)^3} \tag{62}$$

$$Nu = a\,\mathrm{Re}^3 + b\,\mathrm{Re}^2 + c\,\mathrm{Re} + d \tag{63}$$

Thome-Hajal Correlation

This correlation is used for evaporative heat transfer inside the evaporator. The first step is to calculate the thickness of the layer of liquid in the evaporator. Eq. 64 shows how to calculate this.

$$\delta = \frac{D}{4}(1-\gamma) \tag{64}$$

Here δ is the thickness of the liquid layer, D is the diameter of the evaporator, and γ is the void fraction of the refrigerant.

The next step involves the calculation of the heat transfer due to nucleate boiling. Eq. 65 shows the correlation for nucleate boiling while Eq. 66 gives the adaptation for carbon dioxide.

$$h_{nb} = \frac{55 P_r \left[-\log_{10}(P_r)\right]^{-0.55} M^{-0.5} q^{0.67}}{1000} \tag{65}$$

$$h_{nb,CO2} = 0.71 h_{nb} + 3.970 \tag{66}$$

Here h_{nb} is the heat transfer coefficient for nucleate boiling, P_r is the reduced pressure, M is the molar mass of the refrigerant, q is the heat flux, and $h_{nb,CO2}$ is the modified term for carbon dioxide.

Then the contribution of convective boiling must be accounted for. Eq. 67 gives the method of calculating convective boiling.

$$h_{cb} = \frac{0.0133 \,\mathrm{Re}_\ell^{0.69} \,\mathrm{Pr}_\ell^{0.4} \, k_\ell}{\delta} \tag{67}$$

Here h_{cb} is the convective boiling term, Re_ℓ is the liquid Reynolds number, Pr_ℓ is the liquid Prandtl number, and k_ℓ is the thermal conductivity of the saturated liquid.

Because of the fluid flow in the evaporator some of the nucleate boiling is suppressed. The suppression factor, calculated in Eq. 68, accounts for this. Here S is the suppression factor and x is the fluid quality.

$$S = \frac{(1-x)^{0.5}}{0.121\,\mathrm{Re}_{\ell}^{0.225}} \tag{68}$$

Those sections of the pipe wall that are in contact with liquid have their heat transfer capabilities governed by a combination of the convective and nucleate boiling terms. Eq 69 shows how h_{wet} is calculated.

$$h_{wet} = \left[\left(Sh_{nb,CO2} \right)^3 + h_{cb}^3 \right]^{1/3} \tag{69}$$

The proportion of the pipe wall which is actually in contact with the liquid refrigerant must also be calculated. This can be estimated as a simple function of the void fraction of the refrigerant at a given point in the evaporator. Eq. 70 gives the equation for θ_{dry} the angle of the pipe wall that is not in contact with the liquid.

$$\theta_{dry} = \pi + 2\arcsin(2\gamma - 1) \tag{70}$$

With all of this the final two-phase heat transfer coefficient can be calculated. Eq. 71 shows how to calculate h_{tp} the overall two-phase heat transfer. The Gnielinski correlation is used to determine h_{vapor}.

$$h_{tp} = \frac{\theta_{dry} h_{vapor} + \left(2\pi - \theta_{dry} \right) h_{wet}}{2\pi} \tag{71}$$

Yoon et al. Correlation

This correlation is used in the gas cooler when the refrigerant is in a transcritical state. It is simple and consists of two equations. Eq. 72 is used when the temperature of the refrigerant exceeds the critical temperature and Eq. 73 is used if the refrigerant

temperature is below the critical temperature. Here ρ_{cp} is the density of the fluid at the critical point.

$$Nu = 0.013\,\mathrm{Re}\,\mathrm{Pr}^{-0.05}\left(\frac{\rho_{cp}}{\rho}\right)^{1.6} \tag{72}$$

$$Nu = 0.14\,\mathrm{Re}^{0.69}\,\mathrm{Pr}^{0.66} \tag{73}$$

Operating the CO2 System

This appendix provides all the necessary information to maintain and operate the transcritical refrigeration system. Details will follow on charging the system, connecting the system to the data acquisition computer, preparing the system for operation, running the system through Wincon, and saving data for later analysis.

Charging the CO2 system

The first step in adding charge to the transcritical system is to pull a vacuum. This is accomplished using the lab's vacuum pump and manifold which are displayed in Figure 49 and Figure 50 respectively. Figure 51 shows the junction where the CO_2 tank and the manifold should be connected.

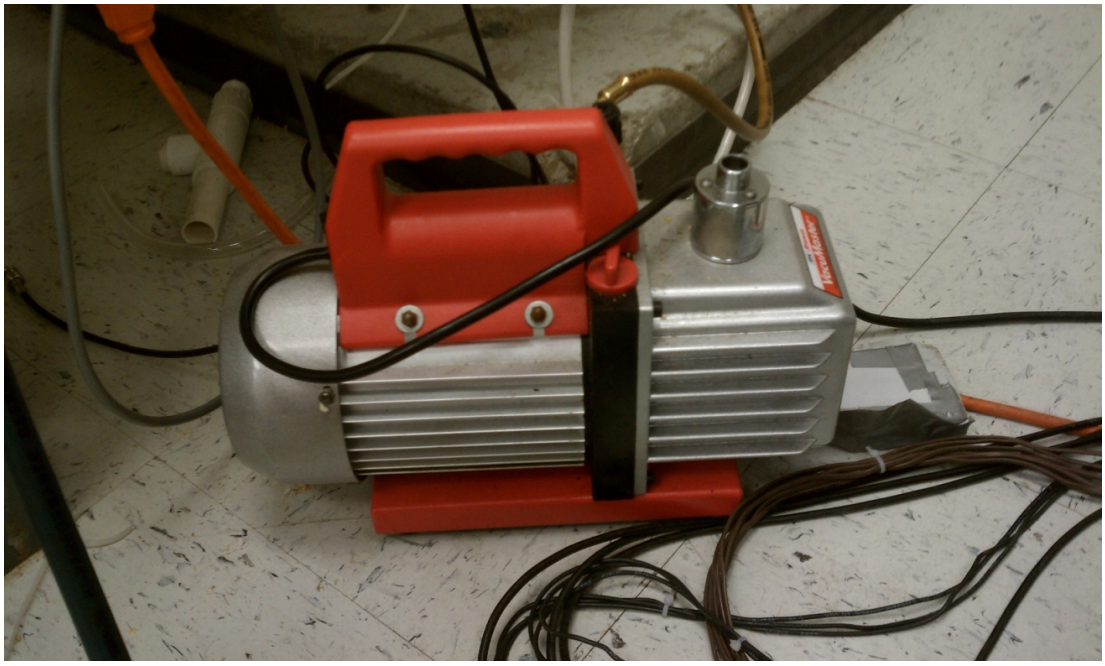

Figure 49. Vacuum pump

Figure 50. Pressure manifold

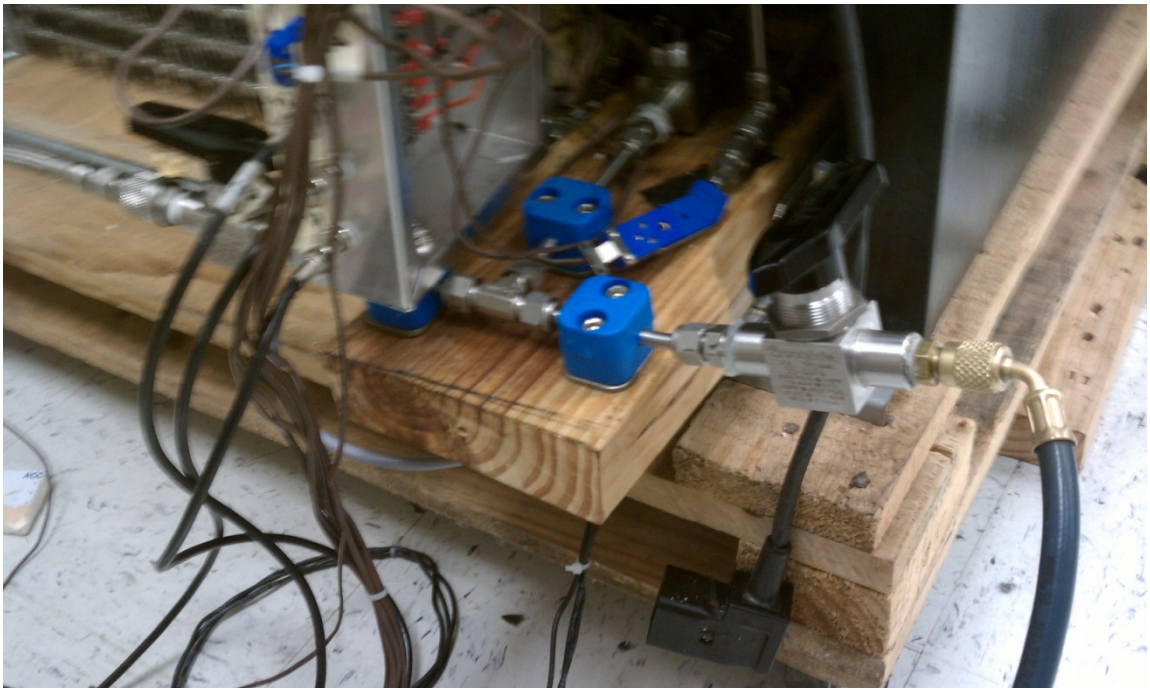

Figure 51. Junction for adding charge

Once this is accomplished, open the regulator valve on either the 10lb or 50lb CO_2 tank. This will allow the addition of charge; however, the pressure in the tank will not be sufficient to fully charge the system. For that you will need to run the system to lower the pressure on the suction side. A scale can be used to ensure the correct amount of charge is added.

Connecting to the DAQ PC

There are a total of eight thermocouple cables and six coaxial cables that will need to be connected to the data acquisition computer before the system can be run. Figure 52 shows the ports for connecting the system. Table 18 details which sensors will be attached to which board.

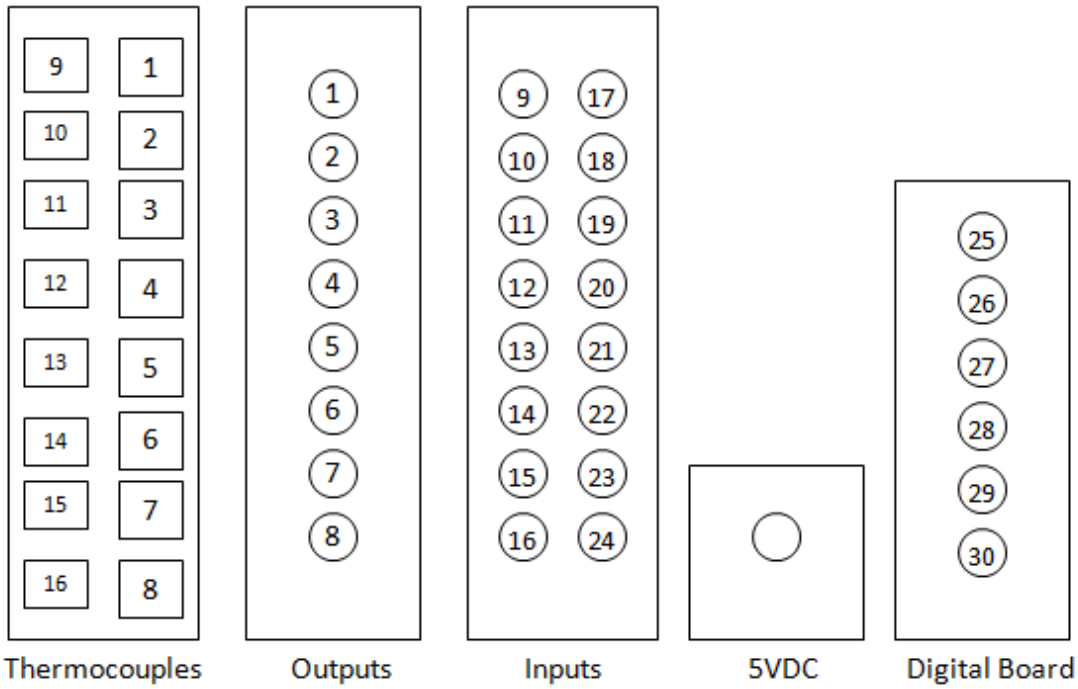

Figure 52. Connections for data acquisition

Table 18. Connections to DAQ PC

Connection	Type	Board	Number
Teai	Thermocouple	Thermocouple	1
Tkro	Thermocouple	Thermocouple	2
Tcro	Thermocouple	Thermocouple	3
Tero	Thermocouple	Thermocouple	4
Tcai	Thermocouple	Thermocouple	5
Teao	Thermocouple	Thermocouple	6
Tcao	Thermocouple	Thermocouple	7
Teri	Thermocouple	Thermocouple	8
EEV	Coaxial	Outputs	4
GC Fan	Coaxial	Outputs	5
Evap Fan	Coaxial	Outputs	6
Pe	Coaxial	Inputs	13
Pgc	Coaxial	Inputs	16
Power	Coaxial	5VDC	NA
Relay	Coaxial	Digital Board	25

Preparing the System

Before running the system, all the powered components must be connected. The 240V connection needs to be attached to its wall socket. For safety reasons, before doing this, go into the hallway and open the circuit breaker panel P1. Flip the 24/26 circuit breaker into the off position, plug in the 240V connection, and then flip the circuit breaker back on.

The other device that needs to be plugged in is the EEV control board. The board is wired to a 24VDC power supply which can be simply connected to any normal wall socket. There is also an on/off switch on the front of the box which must be turned on. If this is left off, the valve will not respond to commands, but instead will remain entirely open. Figure 53 shows the on/off switch on the EEV board.

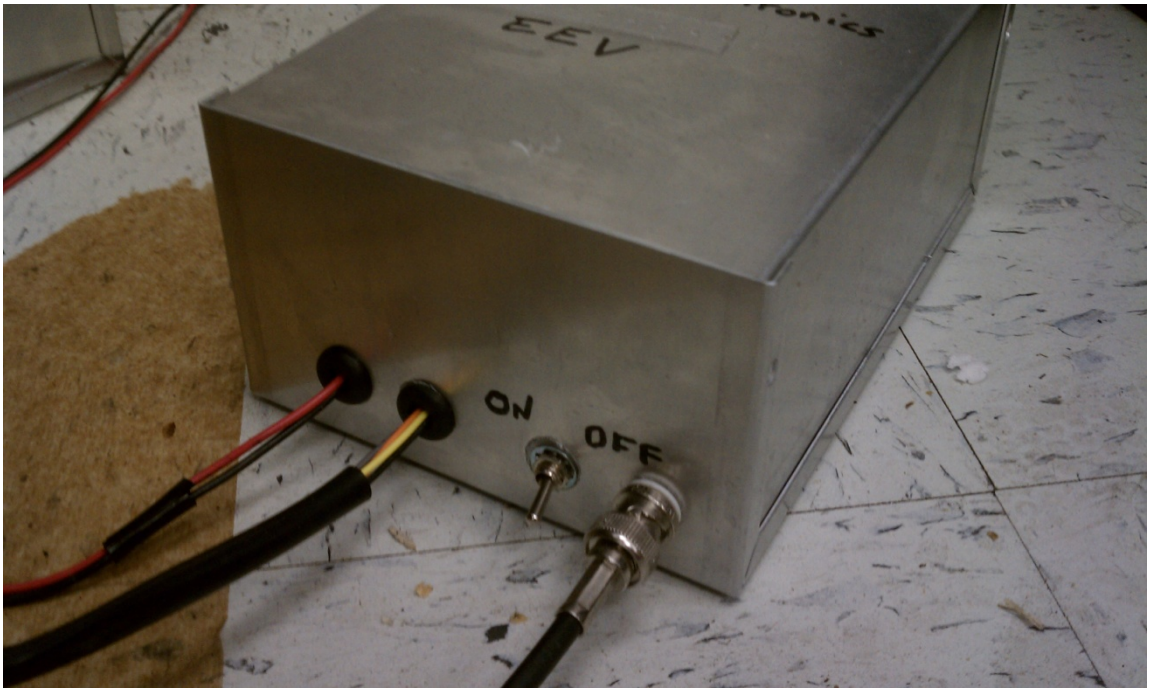

Figure 53. EEV control box

Running Wincon

Control of the system is achieved using Simulink and Wincon. To begin operation start MATLAB. In the MATLAB command window enter 'load FluidProp_CO2' to load the appropriate fluid properties into the workspace. Next the Simulink model which contains the user interface must be opened. While any number of programs can be constructed to accomplish specific tasks, the file 'CO2_sys.mdl' provides manual control of all actuators as well as a cascaded PID control for maintaining superheat with the EEV.

With the Simulink file, open the 'Wincon' menu from the taskbar. Select 'clean' from the drop down menu. This will eliminate any associated old files. Open the 'Wincon' menu again and select 'build'. At this point Wincon will start and prepare a new window for running the system. This new window will have a button to start the system as well as a button to open the scopes present in the Simulink file. This will allow operation of the system.

To save data open the 'Datalog' scope. This contains all input and output signals. Before starting an experiment the 'buffer' of the scope must be adjusted. This governs how many seconds of data will be stored before old data starts to be eliminated. After a test is completed, open the menu and select 'freeze plot' before saving data. This will stop any new data from being acquired. Then the data may be saved as either a .m or .mat file depending on the user's preference.

VITA

Name:	Alex Karl Janecke
Address:	3123 TAMU, College Station, TX, 77843
Email Address:	ajanecke@gmail.com
Education:	B.S., Mechanical Engineering, Texas A&M University, 2009 M.S., Mechanical Engineering, Texas A&M University, 2011